

Accepted Manuscript

Synthesis and evaluation of new pyridyl/pyrazinyl thiourea derivatives:
Neuroprotection against amyloid- β -induced toxicity

Jung-eun Park, Ahmed Elkamhawy, Ahmed H.E. Hassan, Ae Nim Pae, Jiyoun Lee,
Sora Paik, Beoung-Geon Park, Eun Joo Roh



PII: S0223-5234(17)30758-4

DOI: [10.1016/j.ejmech.2017.09.043](https://doi.org/10.1016/j.ejmech.2017.09.043)

Reference: EJMECH 9758

To appear in: *European Journal of Medicinal Chemistry*

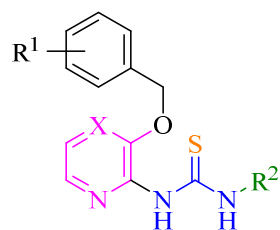
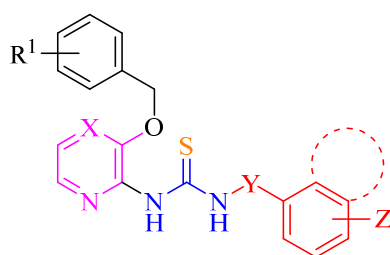
Received Date: 23 August 2017

Revised Date: 20 September 2017

Accepted Date: 21 September 2017

Please cite this article as: J.-e. Park, A. Elkamhawy, A.H.E. Hassan, A.N. Pae, J. Lee, S. Paik, B.-G. Park, E.J. Roh, Synthesis and evaluation of new pyridyl/pyrazinyl thiourea derivatives: Neuroprotection against amyloid- β -induced toxicity, *European Journal of Medicinal Chemistry* (2017), doi: 10.1016/j.ejmech.2017.09.043.

This is a PDF file of an unedited manuscript that has been accepted for publication. As a service to our customers we are providing this early version of the manuscript. The manuscript will undergo copyediting, typesetting, and review of the resulting proof before it is published in its final form. Please note that during the production process errors may be discovered which could affect the content, and all legal disclaimers that apply to the journal pertain.

Graphical Abstract:**Or**

X= CH or N
R¹= H or Various halo-substitutions
R²= Various Aliphatic substitutions
or R²= Y-linked Aryl
Where Y= CH₂ or No atoms
and Z = Various substitution patterns

Designed Small Molecules

ACCEPTED MANUSCRIPT

**Synthesis and evaluation of new pyridyl/pyrazinyl thiourea derivatives:
Neuroprotection against amyloid- β -induced toxicity**

**Jung-eun Park^{a,b,1}, Ahmed Elkamhawy^{a,c,1,*}, Ahmed H. E. Hassan^{d,e}, Ae Nim Pae^{f,g}, Jiyoun Lee^h,
Sora Paik^{a,i}, Beoung-Geon Park^f, Eun Joo Roh^{a,g,*}**

^a Chemical Kinomics Research Center, Korea Institute of Science and Technology (KIST), Seoul 02792, Republic of Korea

^b Department of Chemistry, Sogang University, Seoul 04107, Republic of Korea

^c Department of Pharmaceutical Organic Chemistry, Faculty of Pharmacy, Mansoura University, Mansoura 35516, Egypt

^d Department of Medicinal Chemistry, Faculty of Pharmacy, Mansoura University, Mansoura 35516, Egypt

^e Medicinal Chemistry Laboratory, Department of Pharmacy, College of Pharmacy, Kyung Hee University, Seoul 02447, Republic of Korea

^f Convergence Research Center for Diagnosis, Treatment and Care System of Dementia, Korea Institute of Science and Technology (KIST), Seoul 02792, Republic of Korea

^g Division of Bio-Medical Science & Technology, KIST School, Korea University of Science and Technology, Seoul 02792, Republic of Korea

^h Department of Global Medical Science, Sungshin Women's University, Seoul 142-732, Republic of Korea

ⁱ Department of Fundamental Pharmaceutical Sciences, College of Pharmacy, Kyung Hee University, Seoul, 02447, Republic of Korea

Corresponding authors:

Ahmed Elkamhawy (e-mail: a.elkamhawy@gmail.com) & Eun Joo Roh (e-mail:
r8636@kist.re.kr)

¹ Both authors contributed equally to this work

Abstract

Herein, we report synthesis and evaluation of new twenty six small molecules against β amyloid ($A\beta$)-induced opening of mitochondrial permeability transition pore (mPTP) using JC-1 assay which measures the change of mitochondrial membrane potential ($\Delta\Psi_m$). The neuroprotective effect of seventeen compounds against $A\beta$ -induced mPTP opening was superior to that of the standard Cyclosporin A (CsA). Fifteen derivatives eliciting increased green to red fluorescence percentage less than 40.0% were evaluated for their impact on ATP production, cell viability and neuroprotection against $A\beta$ -induced neuronal cell death. Among evaluated compounds, derivatives **9w**, **9r**, and **9k** had safe profile regarding ATP production and cell viability. In addition, they exhibited significant neuroprotection (69.3, 51.8, and 48.2% respectively). Molecular modeling study using CDocker algorithm predicted plausible binding modes explaining the elicited mPTP blocking activity. Hence, this study suggests compounds **9w**, **9r**, and **9k** as leads for further development of novel therapy to Alzheimer's disease.

Keywords: β -amyloid peptide ($A\beta$); Mitochondrial permeability transition pore (mPTP); $A\beta$ -induced neurotoxicity; Alzheimer's disease (AD); Thiourea; Cyclophilin D; Molecular docking.

1. Introduction

Mitochondria are double-membraned subcellular organelles responsible mainly for vital cellular processes controlling energy production and calcium ions storage. Among subcellular organelles, mitochondria are unique with their high transmembrane potential that could reach up to 180 mV with an internal negative membrane potential [1, 2]. This electric potential across the membrane is essential for the flow of protons through ATP synthase and, hence, ATP generation. It is also the impetus for calcium uptake by mitochondria [3]. A mega channel known as mitochondrial permeability transition pore (mPTP) capable of permeating solutes up to 1500 Da, has been identified across mitochondrial membranes [4]. Under normal physiological conditions, mPTP elicits a low conductance which assists in maintaining the potential across the membrane. In fact; acute mPTP opening under these conditions participates in calcium regulation and cycling [5-7]. Nonetheless, under pathological conditions, aberrant extended opening of mPTP dissipates the mitochondrial membrane potential, resulting in cessation of ATP production, disruption of mitochondrial homeostasis, swelling and rupture of mitochondrial membrane with release of cell death factors [8-11]. As mitochondria are distributed in almost every tissues' cells within the body, detrimental mPTP opening can be manifested in a wide variety of diseases including neurodegenerative diseases, cardiovascular diseases and hepatic diseases [12-22]. Consequently, development of mPTP blockers might be a promising approach for cytoprotection against diseases whose etiology is due to loss of mitochondrial membrane potential [23-26].

Since mPTP discovery in 1979 by Haworth and Hunter [27], there has been a long-lasting debate about its molecular components. The latest accepted model suggests mPTP as a conglomerate of

several molecular subunits with a core formed by dimers of F_0/F_1 ATP synthase. This core is in a direct interaction with cyclophilin D (CypD) in the mitochondrial matrix. Other molecular components of this suggested model include adenine nucleotide translocator (ANT), inorganic phosphate carrier (PiC), mitochondrial creatine kinase (CK), voltage dependent anion channel (VDAC), Bcl-2-associated X protein (Bax) and Bcl-2 homologous antagonist killer (Bak). In addition to these structural elements, regulatory elements have been proposed in this model including mitochondrial translocator protein (TSPO), protein kinase C epsilon (PKC ϵ) and glycogen synthase kinase 3-beta (GSK3- β) [28]. Whether this proposed model or other suggested model is the exact model, it is a fact that CypD has been always an integral component of every suggested mPTP model [29, 30]. In fact, Haworth's discovery of mPTP [27] was confirmed when permeability transition was blocked by the inhibitory effect of cyclosporin A (CsA) on CypD [31, 32].

Despite being an effective mPTP inhibitor, CsA is also a powerful immunosuppressant. This renders it unsuitable as a therapeutic agent for *in vivo* mPTP opening inhibition [33]. Moreover, its polypeptidic structure imparts poor kinetic properties for crossing blood brain barrier (BBB) which hampers its bioavailability to central nervous system neurons [34]. Apparently, the development of non-immunosuppressant small molecule inhibitors of mPTP having good BBB-crossing kinetics could be a viable approach to achieve neuronal cytoprotection and hence prevention of neurodegenerative diseases progression. Actually, non-immunosuppressant analogs of CsA have been developed exemplified by NIM811 and UNIL025. Nevertheless, these polypeptidic molecules suffer from side effects coupled with poor BBB-crossing kinetics which curbs their use in neurological diseases [35, 36].

Reports of efforts to develop mPTP opening modulators are scarce in literature. Among these efforts, Guo *et al.* described a micromolar activity for quinoxaline derivative (**1**) (Fig. 1) as selective inhibitor of CypD over CypA [37]. Rather than this report, no further effort was reported to develop more potent and selective mPTP modulator of quinoxaline scaffold. Also, furamide derivatives (**2**) were reported to inhibit calcium induced mitochondrial swelling, albeit at a high micromolar concentration [38]. The diarylisoxazole-3-carboxamide (**3**) and *N*-phenylbenzamide (**4**) were reported to maintain mitochondrial potential in models of calcium-induced mitochondrial permeability transition. However, they were found to target unconfirmed biological target other than CypD [39, 40]. To the best of our knowledge, the therapeutic small molecule inhibitor of mPTP has not been realized yet. This prompted us to pursue identification of promising mPTP modulators able to achieve neuroprotection and stall progression of neurodegenerative diseases. In a recent report, screening of our institute's internal chemical library using JC-1 assay unveiled quinuclidinyl oxime ether (**5**) as a promising molecule maintaining mitochondrial membrane potential in models of amyloid beta (A β)-induced mPTP opening [41]. Modifications of hit compound **5** resulted in series of pyrrolidinyl triazoles (**6**) and *N*-alkyl-*N'*-pyridyl ureas (**7**) as mPTP inhibitors [42, 43]. In these two series, the linkers might contribute to the elicited affinity.

<Please Insert Fig.1. Here>

CypD bears 75% sequence identity with CypA which is another member of cyclophilin family of peptidyl-prolyl isomerases (PPI). Moreover, the contact surface amino acid residues of human

CypD and CypA with CsA are conserved in both of them [44]. This might be an indication of the usefulness of CypA inhibitors as hits for designing potential promising CypD inhibitors. Compound **8** (Fig. 1) was designed as a CypA inhibitor by linking two hydrophobic aromatic fragments *via* an acylurea linker [45]. In addition, triazole, urea and acylurea linkers of compounds **6**, **7** and **8** respectively might donate and/or accept hydrogen bonds. In fact, the crystal structure of CsA bound to CypD (pdb ID = 2Z6W) discloses favorable hydrogen bonding interactions within the binding cavity between amide groups of CsA and Arg55, Asn102, Trp121 and His126 [44]. Therefore, we envisioned that replacing oxime ether, triazole, urea or acylurea linkers with lipophilic thiourea linker which has stronger tendency to form hydrogen bonding [46], would enable more efficient simulation of some hydrogen bonding interactions pattern of CsA, while improving the biological activity and BBB penetration at the same time. In addition, exploration of the structure activity relationship through replacing the eastern aliphatic moieties of compounds **5** and **6** with different aromatic moieties or aliphatic chains was planned. Moreover, investigations of the impact of retaining the pyridine ring or isosteric replacement with pyrazine ring, in addition to, incorporation of non-halogenated or different halogenated benzyloxy moieties were considered.

2. Results and discussion

2.1. Chemistry

Achieving conciseness of the target molecules' synthetic pathway is one of the ultimate goals in the science of synthesis. The more synthetic steps involved the more attrition of the yield and higher cost of the final compounds. Thereby, ideal synthesis should involve only one high yielding synthetic step. While achieving ideal synthesis remains far from practice in many cases,

it should be an inspiring aim for planning near ideal synthesis. Keeping up these goals, a concise preparation of the target compounds (**9a–z**) was achieved in two synthetic steps starting from commercially available 2-amino-3-hydroxypyridine (**10a**) or 2-amino-3-chloropyrazine (**10b**). While 3-(benzyloxy)pyridine-2-amine (**11a**) is commercially available, other 3-benzyloxy-2-pyridinamines (**11b–d**) were prepared *via* *O*-alkylation of the starting pyridine derivative **10a** with the appropriate benzyl bromide derivative in biphasic medium employing a phase transfer catalyst under basic conditions. For pyrazine derivatives, nucleophilic aromatic substitution of **10b** with the appropriate phenylmethoxide derivative generated by treatment of the corresponding benzyl alcohol with sodium hydride afforded 3-(substituted-benzyloxy)pyrazin-2-amine derivatives (**11e–f**). Nucleophilic addition of intermediates **11** to aromatic isothiocyanate afforded the corresponding 1,3-diarylthioureas. However, for reaction with aliphatic thiourea derivatives, the intermediates **11** were first converted *in situ* to sodium amide derivatives which underwent reaction with the appropriate aliphatic isothiocyanate derivative to afford the targeted 1-alkyl-3-arylthioureas.

<Please Insert Scheme 1. Here>

2.2. Biological evaluation

2.2.1. Protection against loss of mitochondrial membrane potential assay (JC-1 assay)

As highlighted previously, mitochondrial membrane potential ($\Delta\Psi_M$) is crucial for maintaining integrity of mitochondria. Prolonged opening of the mega-channel mPTP results in decay of mitochondrial membrane potential. Mitochondria with maintained membrane potential are featured with an inside negative matrix potential. Consequently, the decline in mitochondrial membrane potential might be quantified using fluorescent cationic dyes. For accurate

measurements, an ideal cationic dye to be used should be affected only by mitochondrial membrane potential without probability to be affected by other factors including the plasma membrane potential ($\Delta\Psi_p$) which would interfere with these measurements. JC-1 (5,5',6,6'-tetrachloro-1,1',3,3'-tetraethylbenzimidazolocarbo-cyanine iodide) is a lipophilic cationic cyanine dye; offers many advantages over other cationic dyes as its performance is specific for the mitochondrial membrane potential. JC-1 is not affected by other components including plasma membrane potential ($\Delta\Psi_p$), mitochondrial size or shape [47, 48]. It self-assembles into red fluorescing aggregates in the matrix of mitochondria having physiologically normal membrane potential. Upon loss of membrane potential, these aggregates break up into green fluorescing monomers. Induction of mPTP opening in presence of compounds to be evaluated as mPTP blockers and measuring the ratio of the red to green fluorescence enables quantification of protective effects of these compounds. Amyloid beta ($A\beta$) is a neurotoxin which plays a crucial role in progression of neurodegeneration. Upon interaction with mitochondria, $A\beta$ triggers mPTP opening with a concomitant loss of membrane potential. Consequently, $A\beta$ -induced mPTP opening model was selected for initial biological evaluation of prepared compounds. In this model, $A\beta$ produced fluorescence shift from red to green as the membrane potential is lost. The protective effect of synthesized target compounds against $A\beta$ -induced potential loss was quantified by measuring the decrement of green to red fluorescence ratio in hippocampal neuronal cells. The results of evaluation are presented in Table 1. The standard CsA lowered the green to red ratio to 46.0%, thus recovering 54.0% of mitochondrial membrane potential.

<Please Insert Table 1. Here>

Twenty six derivatives (**9a–z**) bearing halogenated or non-halogenated benzyloxy moieties of pyridine or pyrazine scaffolds linked to aliphatic or aromatic moieties through a thiourea spacer were synthesized and biologically assessed for their mPTP blocking activity using JC-1 assay. The results of the evaluation are illustrated in Fig. 2. The dashed line across the figure represents the level of green to red ratio elicited by CsA in the course of the employed test. Compounds having values of percentage increase in the fluorescence ratio (green/red) lower than the dashed line are eliciting superior mPTP blocking activity than that of standard CsA, while those compounds whose values of percentage increase in the fluorescence ratio (green/red) above the dashed line are less effective than CsA.

In the beginning, compounds having pyridine scaffold were prepared and evaluated. As shown in Table 1 and illustrated in Fig. 2, all ethyl, *tert*-butyl and benzyl derivatives (**9a**, **9c**, **9d**, **9h**, **9j**, **9l** and **9q**) which bear unsubstituted, 3-fluoro, 2-chloro or 3-chlorobenzyloxy substitution in the western part, were ineffective or having weak efficiency in reducing the green to red fluorescence ratio. The isopropyl derivatives elicited mixed results; while isopropyl derivative **9i** which bears 3-fluorobenzyloxy substitution in the western part was ineffective, the isopropyl derivative **9b** elicited efficacy almost as CsA (45.2% and 46.0% respectively), whereas, the isopropyl derivative **9m** showed better reduction of green to red ratio (31.7%). In contrast to the aliphatic derivatives, all aromatic derivatives having unsubstituted, 3-fluoro, 2-chloro or 3-chlorobenzyloxy substitution in the western part exhibited superior activity than that of CsA in retaining mitochondrial potential. The best performing aromatic derivative **9o** showed increase in the green to red fluorescence ratio around fourth of CsA value (13.0% and 46.0% respectively), while aromatic derivative **9r** which is the least effective among prepared aromatic derivatives is

still more efficient than CsA (38.0% and 46.0% respectively). Out of ten prepared aromatic derivatives, five derivatives (**9g**, **9k**, **9n**, **9o** and **9p**) showed excellent reductions of the increased green to red fluorescence ratio within range of (13.0%~17.5%), while other four derivatives (**9e**, **9f**, **9s** and **9t**) were less efficient, however, still also excellent reductions of the increased green to red fluorescence ratio within range of (23.3%~26.0%).

Next, we explored the performance of derivatives having pyrazine scaffold in JC-1 assay. Six derivatives having isopropyl, *tert*-butyl, benzyl, 4-methylphenyl and 3-chlorophenyl substitutions in eastern part were prepared and evaluated. In paradox to ineffective analogous pyridine derivatives, compounds **9u** and **9v** having pyrazine scaffold, bearing isopropyl and *tert*-butyl substituents in eastern part and 3-fluorobenzyloxy in the western part showed appreciable activities (reduced the percent of increased green to red fluorescence ratio to 43.1 and 28.1% respectively). However, compounds **9x** and **9z** having pyrazine scaffold, bearing isopropyl and 3-chlorophenyl substituents in eastern part and 2-chlorobenzyloxy in the western part were less effective than the analogous pyridine derivatives. The most active compounds prepared among both pyridine and pyrazine series were pyrazine derivatives **9w** and **9y** (reduced the percent of increased green to red fluorescence ratio to 4.6 and 5.3% respectively).

<Please Insert Fig.2. Here>

2.2.2. Assessment of compounds toxic effect on ATP production (Luciferase-based assay) and neurocytotoxicity (MTT assay)

In drug discovery process, it is critical to implement assessment of toxicity early in workflow of the discovery program. These front toxicity assays would filter out likely toxic compounds and thus minimize the probability of developing molecules that would fail later because of their toxicities [49]. As mentioned before, mitochondria are cells' indispensable power-plants generating most of the ATP produced in various tissues of the body. Compounds inducing mitochondrial toxicity would seriously affect normal functioning of cells, and thereby, it is a pivotal issue to be considered for development of safe drugs [50, 51]. In addition to these general concerns in drug development, a special concern arises from the assumed model of mitochondrial permeability transition pore (mPTP) which suggests dimers of ATP synthase as the core element forming the pore. Consequently, it is important to confirm that molecules designed as mPTP blockers do not interfere with normal physiological production of ATP because if ATP synthases were inhibited as a part of mPTP inhibition process, this would deprive cells from the vital process of mitochondrial ATP production. Hence, the most active fifteen derivatives which elicited increased green to red fluorescence percentage less than 40.0% were evaluated for their effect on cellular ATP production in hippocampal neuronal cells. After 7 hours incubation of cells with 5 μ M solution of the tested compound, a luciferase based assay was employed for measurement of ATP in the cells' lysate. As presented in Table 2 and illustrated in Fig. 3, compounds **9e**, **9f**, and **9g** with unsubstituted benzyloxy moiety significantly decreased the levels of ATP. Other tested compounds (**9k**, **9m**, **9n**, **9o**, **9p**, **9r**, **9s**, **9t**, **9v**, **9w**, and **9z**) showed more or less insignificant impact on cellular ATP production. Despite thiourea derivative **9y** which elicited high efficacy in lowering the g/r ratio showed some reduction of ATP production, this reduction is still comparable to that of the standard piracetam (85.1 and 88.0% for **9y** and piracetam respectively).

After excluding the unsubstituted benzyloxy derivatives turned out to possess significant detrimental effects on mitochondrial ATP production, the remaining twelve derivatives were subjected to a subsequent filter to exclude compound(s) possessing cytotoxic effects. Accordingly, the promising twelve derivatives (**9k**, **9m**, **9n**, **9o**, **9p**, **9r**, **9s**, **9t**, **9v**, **9w**, **9y**, and **9z**) were submitted to MTT cell viability assay to assess the level of hippocampal neuronal cells survival after incubation for 24 hours with 5 μ M solutions of tested compounds. The results of MTT assay are presented in Table 2. With exception of compound **9p** whose MTT assay result was approximately similar to reference CsA, the other tested eleven compounds showed superior results than that of CsA. Almost no significant reductions in neuronal cells viability were exerted by these compounds. From the combined excellent performance of compounds passed through the applied two consecutive toxicity filters, it can be assumed that these derivatives are devoid of direct toxic effects on mitochondrial ATP production and cytotoxicity on hippocampal neuronal cells.

<Please Insert Table 2 Here>

<Please Insert Fig. 3. Here>

2.2.3. Protection against A β -induced neuronal cell death

Neurodegenerative diseases are progressive in nature which is a major obstacle in developing effective therapies thereof. The neurodegenerative disease tends to worsen by time as of death of more neuronal cells takes place. The death of neurons in neurodegenerative diseases such as Alzheimer's disease is a consequence of multiple complex mechanisms [52]. However, achieving protection of neurons from A β -induced cells death is one of the ultimate goals in

developing new effective treatments for Alzheimer's disease. At sub-micromolar concentrations $A\beta$ is highly neurocytotoxic. It has been reported that 500 nM concentrations induced substantial neuronal necrosis of cerebellar granule cells within 72-168 hours, while at 1 μ M, substantial cerebellar granule cells death took place rapidly within only 24 hours [53]. Moreover, incubation of hippocampal neurons cell line with 2.5 μ M concentrations of $A\beta$ reduced its viability to around 50.0% [54]. Considering these values of elicited cytotoxicity of $A\beta$, we decided to test the ability of each candidate compound to protect hippocampal neuronal cells, over 24 hours incubation time, from cytotoxic effects of 5 μ M concentrations of $A\beta$ which is double the concentration that produced reduction of hippocampal cells viability to around 50.0%. This highly elevated concentration of $A\beta$ was applied hoping that high selection criteria would reveal potentially effective lead compounds protecting neurons against $A\beta$ -induced cell death even in the presence of high concentrations of toxic $A\beta$. The results of protective effects elicited by evaluated compounds are presented in Table 2 and illustrated in Fig. 3. Under these strict criteria of selection, three compounds (**9w**, **9r**, and **9k**) elicited a decent protection of hippocampal neuronal cells against $A\beta$ -induced neurocytotoxicity (69.3, 51.8, and 48.2% for **9w**, **9r**, and **9k** respectively). These values translate into, for compound **9w** for example, that approximately 70.0% of hippocampal neuronal cells died upon incubation with 5 μ M concentration $A\beta$ are still viable after 24 hours of exposure to this highly toxic concentration of $A\beta$ when compound **9w** is present. Compounds tested other than **9w**, **9r**, and **9k** were less or not effective in protecting cells against $A\beta$ -induced death.

2.2.4. Molecular Modeling Study

To gain insights into the possible causes triggering variations in the activity of tested compounds as mPTP modulators, molecular modeling study was conducted using the reported crystal

structure of CypD-CsA complex (pdb ID = 2Z6W). Analysis of CypD-CsA complex revealed the pivotal role of hydrophobic binding interactions. CsA's methylated valine residue (Mva11) docks into a critical binding pocket 1. Juxtaposed to binding pocket 1, a less hydrophobic pocket 2 is partially filled with the CsA's α -amino-butyric acid residue (Aba2). A saddle separates pocket 1 and pocket 2. On the opposite side, there is a flat hydrophobic surface adjoined to pocket 1 which interacts with CsA's methylated leucine residue side chain (Mle9). Two hydrogen bonds contribute to binding of CsA in the saddle region, another two to the edge of pocket 1, and one to the flattened hydrophobic surface.

CDocker [55, 56] was used to perform flexible docking of the synthesized twenty six derivatives (**9a–z**) followed by refining of the best twenty poses *via in situ* minimizations and calculation of binding and complex energies. The analysis of the results of molecular docking simulations revealed two general patterns for binding of docked compounds which might underlay the elicited biological activity. In the first binding pattern, the hydrophobic pocket 1 of CypD is filled by a hydrophobic moiety of the ligand. The ligands effectively maintained mitochondrial membrane potential elicited strong binding interaction of modes belonging to this pattern. The second binding pattern is characterized by hydrophobic pocket 1 being unoccupied by any moiety of the ligand while the ligand docks above this pocket. The molecular simulation study revealed that ineffective compounds have much less calculated binding interaction for the first binding pattern and/or preference towards the second binding pattern.

The distinctive binding patterns of the thiourea derivative **9w** with the highest efficiency in maintaining mitochondrial membrane potential among tested compounds are illustrated in Fig. 4.

There are three discernible subtypes belonging to the first binding pattern. In binding subtype 1 (Fig. 4A), the aromatic ring of the benzyloxy moiety docks into the hydrophobic pocket 1. For compound **9w**, the best pose within this predicted binding mode, was ranked the second best pose among all retrieved twenty poses in terms of calculated binding energies (-53.34 kcal/mol for binding energy, -50.89 kcal/mol for total binding energy and -3053.63 kcal/mol for ligand-receptor complex energy). In this pose, the phenyl ring of benzyloxy moiety docked into the hydrophobic pocket 1. The pyrazine ring and the thiourea linker are directed towards the saddle region.

The second subtype of binding modes belonging to binding pattern 1 is illustrated in Fig. 4B. This subtype is marked by the central pyrazine ring (or pyridine ring in case of pyridine derivatives) being docked within the hydrophobic pocket 1. For compound **9w**, the pyrazine ring is docked in hydrophobic pocket 1 and the thiourea linker is in interaction with the saddle. By a slight difference in calculated binding energies, the best pose of this subtype of binding mode is ranked over the best pose for subtype 1 (-54.53 kcal/mol for binding energy and -51.48 kcal/mol for total binding energy for subtype 2, while, -53.34 kcal/mol for binding energy and -50.89 kcal/mol for total binding energy for subtype 1). However, the ligand-receptor complex energy of the best pose belonging to subtype 1 is more energetically favored than that of subtype 2 (-3030.32 kcal/mol for complex energy of subtype 2, while, -3053.63 kcal/mol for complex energy of subtype 1). These opposing differences in binding and complex energies may indicate that both poses could contribute to the elicited biological activity of compound **9w**.

<Please Insert Fig. 4. Here>

As illustrated in Fig. 4C, in subtype 3 of binding pattern 1, the eastern substitution on the thiourea linker is docked within the hydrophobic pocket 1. In case of compound **9w**. The thiourea spacer is in favorable interactions with the saddle region. The calculated low energy terms for the best pose belonging to this subtype among calculated poses of compound **9w** (-45.964 kcal/mol for binding energy, -44.2041 kcal/mol for total binding energy and -3053.18 kcal/mol for complex energy) indicates low probability of this pose for its contribution to the elicited biological activity of this derivative.

The second general binding pattern for compound **9w** is depicted in Fig. 4D. In this binding pattern, the hydrophobic pocket 1 remains vacant while the ligand is docked above this pocket. The calculated low binding energies (-48.58 kcal/mol for binding energy, -45.53 kcal/mol for total binding energy and -3056.86 kcal/mol for complex energy) indicate little effect of this binding mode on the activity of compound **9w**. Scrutinizing the different anticipated binding patterns combined with calculated energy terms would attribute the high efficiency of compound **9w** to high contribution of subtypes 1 and 2 of the first general binding pattern.

In contrast, inefficient or compounds with low efficiency to maintain the mitochondrial membrane potential, have propensity for the second general binding pattern and/or less energetically favored poses of the first general binding pattern. This is illustrated by predicted binding poses of compound **9c** which was inefficient in maintaining the mitochondrial membrane potential eliciting 91% of green to red fluorescence. The best calculated poses for binding of compound **9c** with CypD are illustrated in Fig. 5. The best energetically favored pose was of the

second general binding pattern (-45.55 kcal/mol for binding energy, -42.19 kcal/mol for total binding energy and -3047.46 kcal/mol for complex energy) which is, as illustrated in Fig. 5A, characterized by vacant hydrophobic pocket 1.

The next best pose of compound **9c** (Fig. 5B) was of the first general binding pattern subtype 1; in which the aromatic ring of the benzyloxy moiety docks into the hydrophobic pocket 1. For this pose of compound **9c**, in addition to being less favored than the pose of second general binding type, the calculated energy terms (-42.69 kcal/mol for binding energy, -38.39 kcal/mol for total binding energy and -3062.26 kcal/mol for complex energy) are considerably much lower than calculated energy terms for the corresponding poses of the same binding pattern of the effective compounds such as **9w** (-53.34 kcal/mol for binding energy, -50.89 kcal/mol for total binding energy and -3053.63 kcal/mol for complex energy). Consequently, the inefficiency of compound **9c** may be attributed to its tendency to the second general binding mode in addition to its lower calculated binding energies in comparison with that of effective derivatives.

Other subtypes of the first general binding pattern were also detected in calculated poses of compound **9c**, however, with less favorable energetic terms. The pose visualized in Fig. 5C, shows compound **9c** binding mode 1 subtype 2; in which the central pyridine ring docks into the hydrophobic pocket 1. The calculated energetic terms were -41.62 kcal/mol for binding energy, -38.26 kcal/mol for total binding energy and -3047.03 kcal/mol for complex energy. Also binding mode 1 subtype 3; in which the eastern hydrophobic *tert*-butyl moiety docks into the hydrophobic pocket 1, was detected in calculated poses of compound **9c** and is visualized in Fig.

5D. The calculated energy terms for this pose was not high (-40.09 kcal/mol for binding energy, -37.26 kcal/mol for total binding energy and -3043.58 kcal/mol for complex energy).

<Please Insert Fig. 5. Here>

3. Conclusion

In this study, three compounds, **9w**, **9r** and **9k**, have been discovered as new mPTP modulators maintaining mitochondrial membrane potential in models of A β -induced mitochondrial membrane depolarization, and furthermore, protecting neuronal cells effectively against A β -induced cytotoxicity. *In vitro* evaluation of mitochondrial and cellular toxicity indicated absence of both of detrimental effects on the mitochondrial vital process of ATP production, and cytotoxicity for these compounds. Furthermore, the conducted *in silico* molecular docking study provided plausible explanation of their observed mPTP blocking activity. Consequently, this study suggests that compounds **9w**, **9r** and **9k** might be used as a leads for development of new effective therapies to Alzheimer's disease.

4. Experimental

4.1. Chemistry

General: All reactions and manipulations were performed in nitrogen atmosphere using standard Schlenk techniques. The reaction solvents purchased from Aldrich Co., TCI and Alfa and used without any other purification. 3-(Benzyloxy)pyridin-2-amine **11a** has been purchased from Alfa Aesar Co. The NMR spectra were obtained on Bruker Avance 300 or 400. ¹H NMR spectra were referenced to tetramethylsilane ($\delta = 0.00$ ppm) as an internal standard and are reported as

follows: chemical shift, multiplicity (br = broad, s = singlet, d = doublet, t = triplet, dd = doublet of doublet, m = multiplet). Column chromatography was performed on Merck Silica Gel 60 (230–400 mesh) and eluting solvents for all of these chromatographic methods are noted as appropriated-mixed solvent with given volume-to-volume ratios. TLC was carried out using glass sheets pre-coated with silica gel 60 F₂₅₄ purchased by Merk. The purity of samples was determined by analytical HPLC using a Water ACQUITY UPLC (CORTECS™) with C18 column (2.1 mm x 100 mm; 1.6 μm) at temperature 40 °C. HPLC data were recorded using parameters as follows: 0.1% formic acid in water and 0.1% formic acid in methanol and flow rate of 0.3 mL/min. For more details, see supplementary file. High-resolution spectra were performed on Waters ACQUITY UPLC BEH C18 1.7μ-Q-TOF SYNAPT G2-Si High Definition Mass Spectrometry.

4.1.1. 3-(Benzyloxy)pyridin-2-amine derivatives (11b–d)

Compounds **11b–d** have been synthesized as reported by our group in a previous report [43].

4.1.2. General procedure of 3-(benzyloxy)pyrazin-2-amine derivatives (11e and 11f)

Sodium hydride (60% in mineral oil, 0.04 g, 1 mmol) was added to a stirred solution of benzyl alcohol derivative (1 mmol) in anhydrous *N,N*-dimethylformamide (3 mL of DMF) at room temperature and stirring was continued for 1 h. 2-Amino-3-chloropyrazine (**10b**, 0.13 g, 1 mmol) was added to the reaction mixture and the reaction mixture was stirred at 100 °C for 15 h. After cooling, the solvent was evaporated and the residue was partitioned between water and dichloromethane. The organic layer was dried over sodium sulfate anhydrous, filtered, and concentrated. The residue was purified by column chromatography (SiO₂, EA/*n*-Hex = 1/5).

4.1.2.1.1. 3-(3-Fluorobenzoyloxy)pyrazin-2-amine (11e)

Light orange solid, yield: 75.6%, ¹H NMR (400 MHz, DMSO-*d*₆) δ = 5.39 (2H, s, OCH₂Ph), 6.36 (2H, br, NH₂), 7.14 (1H, td, *J* = 2.6 Hz, 9.0 Hz, ArH), 7.25 (1H, d, *J* = 3.1 Hz, ArH), 7.32 (1H, d, *J* = 7.6 Hz, ArH), 7.37-7.44 (2H, m, ArH), 7.49 (1H, d, *J* = 3.1 Hz, ArH).

4.1.2.1.2. 3-(2-Chlorobenzoyloxy)pyrazin-2-amine (11f)

Yellow solid, yield: 87.7%, ¹H NMR (400 MHz, CDCl₃) δ = 4.79 (2H, br, NH₂), 5.51 (2H, s, OCH₂Ph), 7.27-7.30 (2H, m, ArH), 7.41-7.42 (1H, m, ArH), 7.43 (1H, d, *J* = 3.1 Hz, ArH), 7.47-7.49 (1H, m, ArH), 7.58 (1H, d, *J* = 3.1 Hz, ArH).

4.1.3. General procedure of thiourea derivatives (9a-z)

For aliphatic thiourea derivatives (R² = alkyl group); 2-Amino-3-benzyloxy pyridine or pyrazine derivative (0.85 mmol) and sodium hydride (60% in mineral oil, 68 mg, 1.71 mmol) was dissolved in dry THF (5 mL). The isothiocyanate derivative (1.02 mmol) was added and the reaction mixture was refluxed for 5–18 h. After cooling, the reaction mixture was evaporated and the residue was purified by flash column chromatography (SiO₂, EA/*n*-Hex = 1/4). For aromatic thiourea derivatives (R² = aryl group); 2-Amino-3-benzyloxy pyridine or pyrazine derivative (2.5 mmol) and isothiocyanate derivative (3 mmol) were dissolved in dry THF (10 mL) and the reaction mixture was refluxed for 3–6 h. After cooling, the reaction mixture was evaporated and the residue was purified by solidification with cold methanol and filtered to give target compounds.

1-(3-(Benzyloxy)pyridin-2-yl)-3-ethylthiourea (9a)

White solid, yield: 49%, mp: 90.6-91.0 °C, HPLC purity: 6.79 min, 100%, ^1H NMR (400 MHz, CDCl_3) δ = 1.34 (3H, t, J = 7.3 Hz, CH_3), 3.75-3.82 (2H, m, CH_2), 5.15 (2H, s, OCH_2Ph), 6.85 (1H, dd, J = 5.1 Hz, 8.1 Hz, ArH), 7.11 (1H, dd, J = 1.3 Hz, 8.1 Hz, ArH), 7.35-7.42 (5H, m, ArH), 7.75 (1H, dd, J = 1.3 Hz, 5.1 Hz, ArH), 8.58 (1H, s, NH), 11.59 (1H, s, NH). ^{13}C NMR (100.6 MHz, CDCl_3) δ = 14.09, 40.53, 70.83, 117.47, 118.27, 127.43, 128.63, 128.92, 135.05, 136.71, 141.09, 144.39, 179.24. HRMS (ES^+): m/z calculated for $\text{C}_{15}\text{H}_{17}\text{N}_3\text{OS}$: 288.1170 $[\text{M}+\text{H}]^+$. Found 288.1179.

1-(3-(Benzyloxy)pyridin-2-yl)-3-isopropylthiourea (9b)

White solid, yield: 14%, mp: 89.4-95.0 °C, HPLC purity: 7.02 min, 98.31%, ^1H NMR (400 MHz, CDCl_3) δ = 1.35 (6H, d, J = 6.6 Hz, 2CH_3), 4.59-4.60 (1H, m, CH), 5.15 (2H, s, OCH_2Ph), 6.85 (1H, dd, J = 5.1 Hz, 8.1 Hz, ArH), 7.11 (1H, dd, J = 1.3 Hz, 8.1 Hz, ArH), 7.35-7.42 (5H, m, ArH), 7.75 (1H, dd, J = 1.3 Hz, 5.1 Hz, ArH), 8.52 (1H, s, NH), 11.55 (1H, s, NH). ^{13}C NMR (100.6 MHz, CDCl_3) δ = 22.24, 47.63, 70.79, 117.43, 118.25, 127.41, 128.61, 128.91, 135.06, 136.68, 141.07, 144.42, 178.00. HRMS (ES^+): m/z calculated for $\text{C}_{16}\text{H}_{19}\text{N}_3\text{OS}$: 302.1327 $[\text{M}+\text{H}]^+$. Found 302.1331.

1-(3-(Benzyloxy)pyridin-2-yl)-3-(*tert*-butyl)thiourea (9c)

White solid, yield: 70%, mp: 136.5-136.9 °C, HPLC purity: 7.31 min, 96.59%, ^1H NMR (400 MHz, CDCl_3) δ = 1.63 (9H, s, 3CH_3), 5.15 (2H, s, OCH_2Ph), 6.82 (1H, dd, J = 5.1 Hz, 8.0 Hz, ArH), 7.08 (1H, dd, J = 1.1 Hz, 8.0 Hz, ArH), 7.34-7.41 (5H, m, ArH), 7.72 (1H, dd, J = 1.1 Hz, 5.1 Hz, ArH), 8.43 (1H, s, NH), 11.82 (1H, s, NH); ^{13}C NMR (100.6 MHz, CDCl_3) δ = 28.41,

54.03, 70.73, 117.12, 118.15, 127.35, 128.57, 128.90, 135.14, 136.48, 141.00, 144.50, 177.67.

HRMS (ES⁺): m/z calculated for C₁₇H₂₁N₃OS: 316.1483 [M+H]⁺. Found 316.1488.

1-Benzyl-3-(3-(benzyloxy)pyridin-2-yl)thiourea (9d)

Yellow solid, yield: 64%, mp: 122.7-124.3 °C, HPLC purity: 7.24 min, 100%, ¹H NMR (400 MHz, CDCl₃) δ = 5.02 (2H, d, *J* = 5.6 Hz, OCH₂Ph), 5.16 (2H, s, OCH₂Ph), 6.84 (1H, dd, *J* = 5.2 Hz, 8.0 Hz, ArH), 7.11 (1H, dd, *J* = 1.2 Hz, 8.0 Hz, ArH), 7.29-7.30 (1H, m, ArH), 7.34-7.42 (9H, m, ArH), 7.67 (1H, dd, *J* = 5.2 Hz, 8.0 Hz, ArH), 8.69 (1H, s, NH), 12.04 (1H, s, NH). ¹³C NMR (100.6 MHz, CDCl₃) δ = 49.63, 70.89, 117.69, 118.46, 127.47, 127.58, 128.69, 128.95, 135.04, 136.77, 137.58, 141.11, 144.24, 179.98. HRMS (ES⁺): m/z calculated for C₂₀H₁₉N₃OS: 350.1327 [M+H]⁺. Found 350.1329.

1-(3-(Benzyloxy)pyridin-2-yl)-3-(3-chlorophenyl)thiourea (9e)

Yellow solid, yield: 79%, mp: 134.8-135.3 °C, HPLC purity: 7.52 min, 100%, ¹H NMR (400 MHz, CDCl₃) δ = 5.19 (2H, s, OCH₂Ph), 6.94 (1H, dd, *J* = 5.2 Hz, 8.0 Hz, ArH), 7.18-7.22 (2H, m, ArH), 7.32 (1H, t, *J* = 8.0 Hz, ArH), 7.37-7.42 (5H, m, ArH), 7.66 (1H, d, *J* = 8.0 Hz, ArH), 7.79 (1H, t, *J* = 2.0 Hz, ArH), 7.81 (1H, dd, *J* = 1.2 Hz, 5.2 Hz, ArH), 8.76 (1H, s, NH), 13.73 (1H, s, NH). ¹³C NMR (100.6 MHz, CDCl₃) δ = 71.05, 118.16, 118.89, 122.62, 124.39, 126.04, 127.51, 128.78, 129.00, 129.61, 134.16, 134.86, 136.61, 139.99, 141.32, 143.95, 178.44. HRMS (ES⁺): m/z calculated for C₁₉H₁₆ClN₃OS: 370.0781 [M+H]⁺. Found 370.0786.

1-(3-(Benzyloxy)pyridin-2-yl)-3-(4-methylphenyl)thiourea (9f)

Yellow solid, yield: 67%, mp: 106.4-107.2 °C, HPLC purity: 7.42 min, 98.83%, ¹H NMR (400 MHz, CDCl₃) δ = 2.36 (3H, s, CH₃), 5.18 (2H, s, OCH₂Ph), 6.91 (1H, dd, *J* = 5.2 Hz, 8.0 Hz, ArH), 7.16 (1H, dd, *J* = 1.2 Hz, 8.0 Hz, ArH), 7.20 (2H, d, *J* = 8.0 Hz, ArH), 7.36-7.43 (5H, m, ArH), 7.54 (2H, d, *J* = 8.0 Hz, ArH), 7.80 (1H, dd, *J* = 1.2 Hz, 5.2 Hz, ArH), 8.73 (1H, s, NH), 13.47 (1H, s, NH). ¹³C NMR (100.6 MHz, CDCl₃) δ = 21.20, 70.92, 118.10, 118.82, 124.55, 127.56, 128.68, 128.94, 129.35, 135.08, 135.90, 136.31, 136.61, 141.18, 143.92, 178.31. HRMS (ES⁺): *m/z* calculated for C₂₀H₁₉N₃OS: 350.1327 [M+H]⁺. Found 350.1337.

1-(3-(Benzyloxy)pyridin-2-yl)-3-(naphthalen-1-yl)thiourea (9g)

White solid, yield: 49%, mp: 152.0-154.1 °C, HPLC purity: 7.45 min, 90.33%, ¹H NMR (400 MHz, CDCl₃) δ = 5.19 (2H, s, OCH₂Ph), 6.96 (1H, dd, *J* = 5.2 Hz, 8.0 Hz, ArH), 7.22 (1H, dd, *J* = 5.2 Hz, 8.0 Hz, ArH), 7.36-7.44 (5H, m, ArH), 7.50-7.54 (2H, m, ArH), 7.56 (1H, d, *J* = 7.6 Hz, ArH), 7.81-7.83 (2H, m, ArH), 7.89-7.91 (1H, m, ArH), 8.00 (1H, d, *J* = 7.6 Hz, ArH), 8.07-8.09 (1H, m, ArH), 8.92 (1H, s, NH), 13.79 (1H, s, NH). HRMS (ES⁺): *m/z* calculated for C₂₃H₁₉N₃OS: 386.1327 [M+H]⁺. Found 386.1336.

1-(3-(3-Fluorobenzyloxy)pyridin-2-yl)-3-ethylthiourea (9h)

White solid, yield: 49%, mp: 116.2-116.8 °C, HPLC purity: 6.77 min, 100%, ¹H NMR (400 MHz, CDCl₃) δ = 1.34 (3H, t, *J* = 7.2 Hz, CH₃), 3.75-3.82 (2H, m, CH₂), 5.14 (2H, s, OCH₂Ph), 6.86 (1H, dd, *J* = 5.2 Hz, 8.0 Hz, ArH), 7.03-7.09 (3H, m, ArH), 7.17 (1H, d, *J* = 7.2 Hz, ArH), 7.35-7.40 (1H, m, ArH), 7.77 (1H, dd, *J* = 1.2 Hz, 5.2 Hz, ArH), 8.56 (1H, s, NH), 11.56 (1H, s, NH). ¹³C NMR (100.6 MHz, CDCl₃) δ = 14.07, 40.55, 70.03, 114.29 (*J*_{C-F} = 22.1 Hz), 115.61 (*J*_{C-F} = 21.1 Hz), 117.47, 118.27, 122.83 (*J*_{C-F} = 2.0 Hz), 130.64 (*J*_{C-F} = 8.0 Hz), 137.01, 137.57 (*J*_{C-F}

= 7.0 Hz), 140.79, 144.30, 163.00 (J_{C-F} = 247.5 Hz), 179.22. HRMS (ES^+): m/z calculated for $C_{15}H_{16}FN_3OS$: 306.1076 $[M+H]^+$. Found 306.1078.

1-(3-(3-Fluorobenzyloxy)pyridin-2-yl)-3-isopropylthiourea (9i)

White solid, yield: 56%, mp: 131.4-133.2 °C, HPLC purity: 7.00 min, 91.71%, 1H NMR (400 MHz, $CDCl_3$) δ = 1.35 (6H, d, J = 6.8 Hz, 2 CH_3), 4.57-4.61 (1H, m, CH), 5.14 (2H, s, OCH_2Ph), 6.85 (1H, dd, J = 5.2 Hz, 8.0 Hz, ArH), 7.05-7.08 (3H, m, ArH), 7.16 (1H, d, J = 7.6 Hz, ArH), 7.35-7.39 (1H, m, ArH), 7.77 (1H, J = 1.2 Hz, 5.2 Hz, ArH), 8.50 (1H, s, NH), 11.53 (1H, s, NH). ^{13}C NMR (100.6 MHz, $CDCl_3$) δ = 22.23, 47.67, 70.02, 114.27 (J_{C-F} = 22.1 Hz), 115.61 (J_{C-F} = 21.1 Hz), 117.35, 118.21, 122.80 (J_{C-F} = 3.0 Hz), 130.65 (J_{C-F} = 9.1 Hz), 137.00, 137.58 (J_{C-F} = 7.0 Hz), 140.80, 144.41, 163.02 (J_{C-F} = 246.5 Hz), 178.05. HRMS (ES^+): m/z calculated for $C_{16}H_{18}FN_3OS$: 350.1233 $[M+H]^+$. Found 320.1236.

1-(3-(3-Fluorobenzyloxy)pyridin-2-yl)-3-(*tert*-butyl)thiourea (9j)

White solid, yield: 63%, mp: 157.5-159.7 °C, HPLC purity: 7.28 min, 96.35%, 1H NMR (400 MHz, $CDCl_3$) δ = 1.63 (9H, s, 3 CH_3), 5.14 (2H, s, OCH_2Ph), 6.82 (1H, dd, J = 5.2 Hz, 8.0 Hz, ArH), 7.03-7.08 (3H, m, ArH), 7.16 (1H, J = 8.0 Hz, ArH), 7.34-7.39 (1H, m, ArH), 7.74 (1H, dd, J = 1.6 Hz, 5.2 Hz, ArH), 8.40 (1H, s, NH), 11.80 (1H, s, NH). ^{13}C NMR (100.6 MHz, $CDCl_3$) δ = 28.39, 54.07, 69.96, 114.21 (J_{C-F} = 22.1 Hz), 115.55 (J_{C-F} = 21.1 Hz), 117.08, 118.14, 122.75 (J_{C-F} = 3.0 Hz), 130.62 (J_{C-F} = 8.0 Hz), 136.78, 137.66 (J_{C-F} = 8.0 Hz), 140.72, 144.44, 163.01 (J_{C-F} = 247.5 Hz), 177.66. HRMS (ES^+): m/z calculated for $C_{17}H_{20}FN_3OS$: 334.1389 $[M+H]^+$. Found 334.1396.

1-(3-(3-Fluorobenzyloxy)pyridin-2-yl)-3-(naphthalen-1-yl)thiourea (9k)

White solid, yield: 77%, mp: 163.5-166.8 °C, ¹H NMR (400 MHz, CDCl₃) δ = 5.21 (2H, s, OCH₂Ph), 6.96 (1H, dd, *J* = 4.8 Hz, 8.0 Hz, ArH), 7.08-7.09 (1H, m, ArH), 7.10-7.14 (1H, m, ArH), 7.18 (1H, dd, *J* = 1.2 Hz, 8.0 Hz, ArH), 7.22 (1H, d, *J* = 7.6 Hz, ArH), 7.38-7.44 (1H, m, ArH), 7.50-7.54 (2H, m, ArH), 7.57 (1H, d, *J* = 8.0 Hz, ArH), 7.81-7.85 (2H, m, ArH), 7.89-7.91 (1H, m, ArH), 8.00 (1H, d, *J* = 7.6 Hz, ArH), 8.07-8.09 (1H, m, ArH), 8.90 (1H, s, NH), 13.76 (1H, s, NH). ¹³C NMR (100.6 MHz, CDCl₃) δ = 70.22, 114.44 (*J*_{C-F} = 22.1 Hz), 115.76 (*J*_{C-F} = 21.1 Hz), 118.08, 118.84, 122.32, 122.97, 124.43, 125.43, 126.21, 126.64, 127.31, 128.57, 129.26, 130.75 (*J*_{C-F} = 8.6 Hz), 134.27, 134.87, 137.00, 137.46 (*J*_{C-F} = 7.0 Hz), 141.09, 144.19, 163.07 (*J*_{C-F} = 248.5 Hz), 180.00. HRMS (ES⁺): *m/z* calculated for C₂₃H₁₈FN₃OS: 404.1233 [M+H]⁺. Found 404.1238.

1-(3-(2-Chlorobenzyloxy)pyridin-2-yl)-3-ethylthiourea (9l)

Yellow solid, yield: 19%, mp: 98.6-100.2 °C, HPLC purity: 7.02 min, 100%, ¹H NMR (400 MHz, CDCl₃) δ = 1.34 (3H, t, *J* = 7.6 Hz, CH₃), 3.75-3.82 (2H, m, CH₂), 5.25 (2H, s, OCH₂Ph), 6.88 (1H, dd, *J* = 5.2 Hz, 8.0 Hz, ArH), 7.12 (1H, *J* = 1.2 Hz, 8.0 Hz, ArH), 7.28-7.33 (2H, m, ArH), 7.41-7.44 (2H, m, ArH), 7.78 (1H, dd, *J* = 1.2 Hz, 5.2 Hz, ArH), 8.59 (1H, s, NH), 11.58 (1H, s, NH). ¹³C NMR (100.6 MHz, CDCl₃) δ = 14.09, 40.57, 67.99, 117.54, 118.36, 127.36, 129.01, 129.79, 129.87, 132.67, 132.95, 137.05, 140.82, 144.36, 179.24. HRMS (ES⁺): *m/z* calculated for C₁₅H₁₆ClN₃OS: 322.0781 [M+H]⁺. Found 322.0790.

1-(3-(2-Chlorobenzyloxy)pyridin-2-yl)-3-isopropylthiourea (9m)

Yellow solid, yield: 72.3%, mp: 72.5-73.8 °C, HPLC purity: 7.21 min, 93.24%, ¹H NMR (400 MHz, CDCl₃) δ = 1.36 (6H, d, *J* = 6.8 Hz, 2CH₃), 4.57-4.63 (1H, m, CH), 5.25 (2H, s, OCH₂Ph), 6.87 (1H, dd, *J* = 5.2 Hz, 8.0 Hz, ArH), 7.11 (1H, d, *J* = 8.0 Hz, ArH), 7.29-7.33 (2H, m, ArH), 7.41-7.44 (2H, m, ArH), 7.78 (1H, d, *J* = 5.2 Hz, ArH), 8.53 (1H, s, NH), 11.54 (1H, s, NH). ¹³C NMR (100.6 MHz, CDCl₃) δ = 22.23, 47.63, 67.98, 117.53, 118.37, 127.30, 129.03, 129.74, 129.85, 132.64, 132.96, 137.02, 140.74, 144.32, 178.00. HRMS (ES⁺): *m/z* calculated for C₁₆H₁₈ClN₃OS: 336.0937 [M+H]⁺. Found 336.0945.

1-(3-(2-Chlorobenzoyloxy)pyridin-2-yl)-3-(3-chlorophenyl)thiourea (9n)

Yellow solid, yield: 83%, mp: 127.8-128.5 °C, HPLC purity: 7.70 min, 100%, ¹H NMR (400 MHz, CDCl₃) δ = 5.29 (2H, s, OCH₂Ph), 6.94 (1H, dd, *J* = 5.2 Hz, 8.0 Hz, ArH), 7.10-7.12 (1H, m, ArH), 7.19-7.35 (4H, m, ArH), 7.43-7.46 (2H, m, ArH), 7.66 (1H, d, *J* = 8.0 Hz, ArH), 7.78 (1H, t, *J* = 2.4 Hz, ArH), 7.85 (1H, dd, *J* = 1.2 Hz, 5.2 Hz, ArH), 8.76 (1H, s, NH), 13.72 (1H, s, NH). ¹³C NMR (100.6 MHz, CDCl₃) δ = 68.27, 118.23, 119.03, 122.60, 124.38, 126.05, 127.40, 129.17, 129.62, 129.88, 130.04, 132.48, 133.12, 134.16, 136.95, 139.97, 141.06, 143.92, 178.44. HRMS (ES⁺): *m/z* calculated for C₁₉H₁₅Cl₂N₃OS: 404.0391 [M+H]⁺. Found 404.0397.

1-(3-(2-Chlorobenzoyloxy)pyridin-2-yl)-3-(4-methylphenyl)thiourea (9o)

Yellow solid, yield: 15%, mp: 138.9-142.7 °C, HPLC purity: 7.58 min, 91.48%, ¹H NMR (400 MHz, CDCl₃) δ = 2.36 (3H, s, CH₃), 5.29 (2H, s, OCH₂Ph), 6.92 (1H, dd, *J* = 5.2 Hz, 8.0 Hz, ArH), 7.07-7.14 (3H, m, ArH), 7.18-7.19 (1H, m, ArH), 7.21 (2H, d, *J* = 8.0 Hz, ArH), 7.38-7.40 (1H, m, ArH), 7.54 (2H, d, *J* = 8.0 Hz, ArH), 7.82 (1H, dd, *J* = 1.2 Hz, 5.2 Hz, ArH), 8.74 (1H, s, NH), 13.47 (1H, s, NH). ¹³C NMR (100.6 MHz, CDCl₃) δ = 21.11, 68.12, 117.88, 118.71,

124.90, 127.41, 129.09, 129.35, 129.84, 129.96, 132.57, 133.02, 136.13, 136.21, 137.00, 141.02, 144.14, 178.73. HRMS (ES⁺): m/z calculated for C₂₀H₁₈ClN₃OS: 384.0937 [M+H]⁺. Found 384.0947.

1-(3-(2-Chlorobenzyloxy)pyridin-2-yl)-3-(naphthalen-1-yl)thiourea (9p)

White solid, yield: 87%, mp: 116.5-117.3 °C, HPLC purity: 7.63 min, 94.06%, ¹H NMR (400 MHz, CDCl₃) δ = 5.33 (2H, s, OCH₂Ph), 6.96 (1H, dd, *J* = 4.8 Hz, 8.0 Hz, ArH), 7.22-7.25 (2H, m, ArH), 7.34-7.35 (2H, m, ArH), 7.43-7.49 (2H, m, ArH), 7.50-7.58 (3H, m, ArH), 7.82 (1H, d, *J* = 8.0 Hz, ArH), 7.86 (1H, dd, *J* = 1.2 Hz, 5.2 Hz, ArH), 7.89-7.91 (1H, m, ArH), 8.0 (1H, d, *J* = 6.0 Hz, ArH), 8.07-8.10 (1H, m, ArH), 8.92 (1H, s, NH), 13.78 (1H, s, NH). ¹³C NMR (100.6 MHz, CDCl₃) δ = 68.24, 118.17, 118.96, 122.32, 122.69, 123.49, 124.37, 125.44, 126.21, 126.63, 127.16, 127.26, 127.43, 127.76, 128.52, 129.24, 129.97, 132.86, 134.59, 137.03, 141.10, 144.20, 179.99. HRMS (ES⁺): m/z calculated for C₂₃H₁₈ClN₃OS: 420.0937 [M+H]⁺. Found 420.0950.

1-(3-(3-Chlorobenzyloxy)pyridin-2-yl)-3-(*tert*-butyl)thiourea (9q)

White solid, yield: 67%, mp: 128.1-128.6 °C, HPLC purity: 7.47 min, 99.00%, ¹H NMR (400 MHz, CDCl₃) δ = 1.63 (9H, s, 3CH₃), 5.12 (2H, s, OCH₂Ph), 6.83 (1H, dd, *J* = 5.2 Hz, 8.0 Hz, ArH), 7.03 (1H, *J* = 1.2 Hz, 8.0 Hz, ArH), 7.27-7.28 (1H, m, ArH), 7.32-7.35 (3H, m, ArH), 7.73 (1H, dd, *J* = 1.2 Hz, 5.2 Hz, ArH), 8.39 (1H, s, NH), 11.80 (1H, s, NH). ¹³C NMR (100.6 MHz, CDCl₃) δ = 28.39, 54.07, 69.92, 117.09, 118.13, 125.34, 127.35, 128.79, 130.31, 134.82, 136.81, 137.18, 140.69, 144.43, 177.65. HRMS (ES⁺): m/z calculated for C₁₇H₂₀ClN₃OS: 350.1094 [M+H]⁺. Found 350.1102.

1-(3-(3-Chlorobenzyloxy)pyridin-2-yl)-3-(3-chlorophenyl)thiourea (9r)

White solid, yield: 78%, mp: 115.9-117.5 °C, HPLC purity: 7.66 min, 100%, ¹H NMR (400 MHz, CDCl₃) δ = 5.16 (2H, s, OCH₂Ph), 6.94 (1H, dd, *J* = 5.2 Hz, 8.0 Hz, ArH), 7.15 (1H, *J* = 1.2 Hz, 5.2 Hz, ArH), 7.20-7.23 (1H, m, ArH), 7.30-7.38 (5H, m, ArH), 7.64-7.67 (1H, m, ArH), 7.78 (1H, t, *J* = 2.0 Hz, ArH), 7.84 (1H, dd, *J* = 1.2 Hz, 5.2 Hz, ArH), 8.72 (1H, s, NH), 13.70 (1H, s, NH). ¹³C NMR (100.6 MHz, CDCl₃) δ = 70.21, 118.16, 118.87, 122.59, 124.37, 125.50, 126.07, 127.52, 128.99, 129.63, 130.40, 134.71, 134.91, 136.89, 136.93, 139.94, 141.02, 143.88, 178.41. HRMS (ES⁺): *m/z* calculated for C₁₉H₁₅Cl₂N₃OS: 404.0391 [M+H]⁺. Found 404.0394.

1-(3-(3-Chlorobenzyloxy)pyridin-2-yl)-3-(4-methylphenyl)thiourea (9s)

Yellow solid, yield: 21%, mp: 127.1-127.5 °C, HPLC purity: 7.54 min, 100%, ¹H NMR (400 MHz, CDCl₃) δ = 2.36 (3H, s, CH₃), 5.15 (2H, s, OCH₂Ph), 6.91 (1H, dd, *J* = 4.8 Hz, 8.0 Hz, ArH), 7.12 (1H, dd, *J* = 1.2 Hz, 8.0 Hz, ArH), 7.21 (2H, d, *J* = 8.4 Hz, ArH), 7.29-7.31 (1H, m, ArH), 7.35-7.38 (3H, m, ArH), 7.54 (2H, d, *J* = 8.4 Hz, ArH), 7.82 (1H, dd, *J* = 1.2 Hz, 4.8 Hz, ArH), 8.70 (1H, s, NH), 13.45 (1H, s, NH). ¹³C NMR (100.6 MHz, CDCl₃) δ = 21.22, 70.13, 117.84, 118.61, 124.84, 125.50, 127.52, 128.95, 129.35, 130.38, 134.89, 136.13, 136.19, 136.98, 140.97, 144.07, 178.64. HRMS (ES⁺): *m/z* calculated for C₂₀H₁₈ClN₃OS: 384.0937 [M+H]⁺. Found 384.0953.

1-(3-(3-Chlorobenzyloxy)pyridin-2-yl)-3-(naphthalen-1-yl)thiourea (9t)

White solid, yield: 90%, mp: 153.0-154.1 °C, ¹H NMR (400 MHz, CDCl₃) δ = 5.19 (2H, s, OCH₂Ph), 6.96 (1H, dd, *J* = 5.2 Hz, 8.0 Hz, ArH), 7.18 (1H, dd, *J* = 1.2 Hz, 8.0 Hz, ArH), 7.33-7.41 (4H, m, ArH), 7.50-7.54 (2H, m, ArH), 7.57 (1H, d, *J* = 7.6 Hz, ArH), 7.81-7.85 (2H, m,

ArH), 7.89-7.91 (1H, m, ArH), 7.80 (1H, d, $J = 7.2$ Hz, ArH), 7.07-7.09 (1H, m, ArH), 8.89 (1H, s, NH), 13.76 (1H, s, NH). ^{13}C NMR (100.6 MHz, CDCl_3) $\delta = 70.20, 118.05, 118.81, 122.30, 124.42, 125.42, 125.56, 126.19, 126.62, 127.29, 127.57, 128.55, 129.98, 129.25, 130.41, 134.25, 134.85, 134.91, 136.96, 137.02, 141.07, 144.18, 180.02$. HRMS (ES^+): m/z calculated for $\text{C}_{23}\text{H}_{18}\text{ClN}_3\text{OS}$: 420.0937 $[\text{M}+\text{H}]^+$. Found 420.0946.

1-(3-(3-Fluorobenzyloxy)pyrazin-2-yl)-3-isopropylthiourea (9u)

White solid, yield: 69%, mp: 91.0-91.8 °C, HPLC purity: 7.21 min, 98.75%, ^1H NMR (300 MHz, CDCl_3) $\delta = 1.35$ (6H, d, $J = 4.2$ Hz, 2 CH_3), 4.50-4.63 (1H, m, CH), 5.44 (2H, s, OCH_2Ph), 7.01-7.07 (1H, m, ArH), 7.13 (1H, dt, $J = 2.1$ Hz, 9.3 Hz, ArH), 7.20 (1H, d, $J = 7.5$ Hz, ArH), 7.32-7.39 (1H, m, ArH), 7.68 (2H, dd, $J = 3.3$ Hz, 6.0 Hz, ArH), 8.39 (1H, s, NH), 11.00 (1H, s, NH). ^{13}C NMR (100.6 MHz, CDCl_3) $\delta = 22.09, 47.94, 67.96, 115.43$ ($J_{\text{C-F}} = 21.7$ Hz), 115.56 ($J_{\text{C-F}} = 21.0$ Hz), 124.02, 130.33 ($J_{\text{C-F}} = 8.0$ Hz), 131.49, 132.73, 137.78, 139.67, 147.30, 162.45 ($J_{\text{C-F}} = 246.8$ Hz), 178.13. HRMS (ES^+): m/z calculated for $\text{C}_{15}\text{H}_{17}\text{FN}_4\text{OS}$: 321.1185 $[\text{M}+\text{H}]^+$. Found 321.1194.

1-(3-(3-Fluorobenzyloxy)pyrazin-2-yl)-3-(*tert*-butyl)thiourea (9v)

White solid, yield: 81%, mp: 114.5-115.2 °C, HPLC purity: 7.49 min, 100%, ^1H NMR (300 MHz, CDCl_3) $\delta = 1.61$ (9H, s, 3 CH_3), 5.44 (2H, s, OCH_2Ph), 7.01-7.06 (1H, m, ArH), 7.13 (1H, d, $J = 9.0$ Hz, ArH), 7.19-7.29 (1H, m, ArH), 7.31-7.38 (1H, m, ArH), 7.65 (1H, d, $J = 3.0$ Hz, ArH), 7.67 (1H, d, $J = 3.0$ Hz, ArH), 8.28 (1H, s, NH), 11.27 (1H, s, NH). ^{13}C NMR (100.6 MHz, CDCl_3) $\delta = 28.21, 54.47, 67.85, 115.32$ ($J_{\text{C-F}} = 15.1$ Hz), 115.52 ($J_{\text{C-F}} = 13.1$ Hz), 123.92, 130.29 ($J_{\text{C-F}} = 8.0$ Hz), 131.30, 132.37, 137.82 ($J_{\text{C-F}} = 8.0$ Hz), 139.70, 147.21, 162.82 ($J_{\text{C-F}} =$

246.5 Hz), 177.66. HRMS (ES⁺): m/z calculated for C₁₆H₁₉FN₄OS: 335.1342 [M+H]⁺. Found 335.1353.

1-(3-(3-Fluorobenzyloxy)pyrazin-2-yl)-3-(4-methylphenyl)thiourea (9w)

Yellow solid, yield: 44%, mp: 97.6-98.7 °C, ¹H NMR (300 MHz, CDCl₃) δ = 1.50 (3H, s, CH₃), 5.59 (2H, s, OCH₂Ph), 7.27-7.36 (4H, m, ArH), 7.44-7.49 (2H, m, ArH), 7.62 (1H, d, *J* = 7.5 Hz, ArH), 7.74-7.77 (2H, m, ArH), 7.81 (1H, d, *J* = 3.0 Hz, ArH), 8.63 (1H, s, NH), 13.09 (1H, s, NH). ¹³C NMR (100.6 MHz, CDCl₃) δ = 21.13, 68.14, 115.46 (*J*_{C-F} = 15.1 Hz), 115.67 (*J*_{C-F} = 14.1 Hz), 124.08, 124.77, 129.44, 130.39 (*J*_{C-F} = 8.0 Hz), 131.45, 133.21, 135.75, 136.53, 130.67 (*J*_{C-F} = 7.0 Hz), 135.35, 147.42, 162.84 (*J*_{C-F} = 247.5 Hz), 178.66. HRMS (ES⁺): m/z calculated for C₁₉H₁₇FN₄OS: 369.1185 [M+H]⁺. Found 369.1198.

1-(3-(2-Chlorobenzyloxy)pyrazin-2-yl)-3-isopropylthiourea (9x)

Yellow solid, yield: 59%, mp: 116.5-117.8 °C, HPLC purity: 7.44 min, 100%, ¹H NMR (400 MHz, CDCl₃) δ = 1.35 (6H, d, *J* = 6.8 Hz, 2CH₃), 4.55-4.60 (1H, m, CH), 5.55 (2H, s, OCH₂Ph), 7.28-7.32 (2H, m, ArH), 7.42-7.45 (2H, m, ArH), 7.69 (1H, d, *J* = 3.2 Hz, ArH), 7.70 (1H, d, *J* = 3.2 Hz, ArH), 8.40 (1H, s, NH), 11.06 (1H, s, NH). ¹³C NMR (100.6 MHz, CDCl₃) δ = 22.10, 47.92, 66.31, 127.03, 129.81, 129.94, 130.14, 131.45, 132.82, 132.97, 133.98, 139.65, 147.36, 178.13. HRMS (ES⁺): m/z calculated for C₁₅H₁₇ClN₄OS: 337.0890 [M+H]⁺. Found 337.0898.

1-Benzyl-3-(3-(2-chlorobenzyloxy)pyrazin-2-yl)thiourea (9y)

Yellow oil, yield: 37%, HPLC purity: 7.63 min, 100%, ¹H NMR (400 MHz, CDCl₃) δ = 4.99 (2H, d, *J* = 5.2 Hz, OCH₂Ph), 5.56 (2H, s, OCH₂Ph), 7.29-7.33 (3H, m, ArH), 7.34-7.41 (4H, m,

ArH), 7.43-7.46 (2H, m, ArH), 7.62 (1H, d, $J = 3.2$ Hz, ArH), 7.71 (1H, d, $J = 3.2$ Hz, ArH), 8.56 (1H, s, NH), 11.50 (1H, s, NH). HRMS (ES⁺): m/z calculated for C₁₉H₁₇ClN₄OS: 385.0890 [M+H]⁺. Found 385.0896.

1-(3-(2-Chlorobenzyloxy)pyrazin-2-yl)-3-(3-chlorophenyl)thiourea (9z)

Yellow oil, yield: 12%, ¹H NMR (400 MHz, CDCl₃) $\delta = 5.60$ (2H, s, OCH₂Ph), 7.22-7.25 (1H, m, ArH), 7.31-7.35 (3H, m, ArH), 7.44-7.49 (2H, m, ArH), 7.62 (1H, d, $J = 7.6$ Hz, ArH), 7.75-7.76 (2H, m, ArH), 7.81 (1H, d, $J = 3.2$ Hz, ArH), 8.63 (1H, s, NH), 13.09 (1H, s, NH).

4.2. Biological evaluation

4.2.1. Cell culture

HT-22 (mouse hippocampal cells) cells were grown in Dulbecco's Modified Eagle's Medium (DMEM, GIBCO) supplemented with 10% (v/v) FBS and antibiotics (100 μ g/mL penicillin/streptomycin mix) in a humidified atmosphere at 37 °C with 5% CO₂.

4.2.2. Protection against loss of mitochondrial membrane potential (JC-1 assay)

HT-22 cells (30,000 per well) were seeded into a clear 96-well plate (FALCON) at 200 μ L per well one day prior to assay. 750 μ M of JC-1 (Stratagene) in DMSO stock solution was dissolved into phenol red-free Opti-MEM (GIBCO) medium to make final concentration of 7.5 μ M JC-1 per well. Medium was removed from the plate, and 100 μ L per well of JC-1 was added. Plates were incubated for 1 h and 15 min at 37 °C and washed twice with 100 μ L per well PBS. Subsequently, cells were treated with 25 μ L solution of each compound at 5 μ M in Opti-MEM and incubated at 37 °C for 10 min followed by addition of 25 μ L of A β (American peptide, 1–

42) solution at 5 μ M. Fluorescence was measured at every 1 h for 3 h at ex/em 530 nm/580 nm ('red') and ex/em 485 nm/530 nm ('green'). The ratio of green to red fluorescence was recorded and the percent changes in ratio from each compound were calculated and normalized using vehicle control as 100%.

4.2.3. Impact on level of ATP production (Luciferase-based assay)

10,000 HT-22 cells per well were seeded into a clear 96-well plate (FALCON) at 200 μ L per well one day prior to assay. Medium was removed from the plate, and cells were treated with 25 μ L solution of each compound at 5 μ M. Cells were incubated at 37 °C for 7 h and washed twice with PBS. Cells were lysed by using 1% Triton-X 100 in TBST buffer solution and protein concentrations of each well were determined via BCA protein determination kit (Thermo scientific). Equal amount of cell lysates from each well were plated into a white 96-well plate (NUNC) and the amount of ATP levels in each sample was determined by using ATP determination kit (Invitrogen). The ATP levels of each sample were subtracted with vehicle control and percent inhibition were calculated based on the ATP levels of the vehicle control.

4.2.4. Assessment of cytotoxicity (Cell viability MTT assay)

5000 HT-22 cells per well were seeded and treated as above described method. Cells were incubated at 37 °C for 24 h. 10 μ L of MTT solution (3-(4,5-Dimethylthiazol-2-yl)-2,5-diphenyltetrazolium bromide, MTT, Sigma) was added directly to each well and incubated at 37 °C for 2 h. After confirming the formation of blue formazan precipitates under microscope, 140 μ L of solubilizing solution (10% Triton-X 100 in isopropanol with 0.1 M HCl) was added to each well and incubate for another hour at room temperature. Absorbance at 570 nm was

measured and OD values from each well were subtracted with vehicle control and cell viability was calculated.

4.2.5. Protection against A β -induced neurotoxicity

5000 HT-22 cells per well were seeded into a clear 96-well plate (FALCON) at 200 μ L per well one day prior to assay. Medium was removed from the plate, and cells were treated with 25 μ L solution of each compound at 10 μ M and incubated at 37 $^{\circ}$ C for 10 min followed by addition of 25 μ L of amyloid Beta (American peptide, 1–42) solution at 10 μ M. Cells were incubated at 37 $^{\circ}$ C for 24 h. 10 μ L of MTT solution (Thiazolyl blue tetrazolium bromide, Sigma) was added directly to each well and incubated at 37 $^{\circ}$ C for 2 h. After confirming the formation of blue formazan precipitates under microscope, 140 μ L of solubilizing solution (10% Triton-X 100 in Isopropanol with 0.1 M HCl) was added to each well followed by incubation for another hour at room temperature. Absorbance at 570 nm was measured and OD values from each well were subtracted with vehicle control and percent protection was calculated based on using the levels of the vehicle control treated with amyloid Beta as 0% and vehicle control using vehicle control only as 100%.

4.2.6. Molecular Docking

The 3-D coordinates of human cyclophilin D-cyclosporin A complex (pdb code: **2Z6W**) was downloaded from protein databank (<http://www.rcsb.org>). The receptor was treated with protein preparation tool applying default values as implemented in Discovery Studio 4.0 (Accelrys, San Diego, CA, USA). The binding site was defined based on contacts of cyclosporin A with cyclophilin D. Ligands were sketched as 2D structures using ChemBioDraw software then

converted into minimized 3D structures by Ligand Preparation tool implemented in Discovery Studio 4.0. CDocker algorithm (Discovery Studio 4.0) was used to perform docking minimization of the ligands into the defined binding site. The retrieved docked poses were submitted to *in situ* ligand minimization within the binding pocket to calculate the binding energy and complex energy of each pose. The results were visualized and analyzed using tools implemented in Discovery Studio 4.0.

Acknowledgments

This work was supported by the KIST Institutional programs (Grant No. 2E27000) from Korea Institute of Science and Technology and by the Creative Fusion Research Program through the Creative Allied Project funded by the National Research Council of Science & Technology (CAP-12-1-KIST).

References

- [1] A. Szewczyk, L. Wojtczak, Mitochondria as a Pharmacological Target, *Pharmacological Reviews*, 54 (2002) 101-127.
- [2] M.R. Duchon, Roles of Mitochondria in Health and Disease, *Diabetes*, 53 (2004) S96-S102.
- [3] E.J. Griffiths, Mitochondria — potential role in cell life and death, *Cardiovascular Research*, 46 (2000) 24-27.
- [4] A. Vianello, V. Casolo, E. Petrusa, C. Peresson, S. Patui, A. Bertolini, S. Passamonti, E. Braidot, M. Zancani, The mitochondrial permeability transition pore (PTP) — An example of multiple molecular exaptation?, *Biochimica et Biophysica Acta (BBA) - Bioenergetics*, 1817 (2012) 2072-2086.
- [5] C. Brenner, M. Moulin, Physiological roles of the permeability transition pore, *Circulation research*, 111 (2012) 1237-1247.
- [6] J.Q. Kwong, J.D. Molkenin, Physiological and pathological roles of the mitochondrial permeability transition pore in the heart, *Cell metabolism*, 21 (2015) 206-214.
- [7] S.S. Smaili, J.T. Russell, Permeability transition pore regulates both mitochondrial membrane potential and agonist-evoked Ca²⁺ signals in oligodendrocyte progenitors, *Cell calcium*, 26 (1999) 121-130.
- [8] J. Henry-Mowatt, C. Dive, J.-C. Martinou, D. James, Role of mitochondrial membrane permeabilization in apoptosis and cancer, *Oncogene*, 23 (2004) 2850-2860.

- [9] S. Javadov, M. Karmazyn, Mitochondrial Permeability Transition Pore Opening as an Endpoint to Initiate Cell Death and as a Putative Target for Cardioprotection, *Cellular Physiology and Biochemistry*, 20 (2007) 1-22.
- [10] G. Kroemer, L. Galluzzi, C. Brenner, Mitochondrial membrane permeabilization in cell death, *Physiological reviews*, 87 (2007) 99-163.
- [11] J.J. Lemasters, A.-L. Nieminen, T. Qian, L.C. Trost, S.P. Elmore, Y. Nishimura, R.A. Crowe, W.E. Cascio, C.A. Bradham, D.A. Brenner, B. Herman, The mitochondrial permeability transition in cell death: a common mechanism in necrosis, apoptosis and autophagy, *Biochimica et Biophysica Acta (BBA) - Bioenergetics*, 1366 (1998) 177-196.
- [12] A.P. Halestrap, P. Pasdois, The role of the mitochondrial permeability transition pore in heart disease, *Biochimica et Biophysica Acta (BBA) - Bioenergetics*, 1787 (2009) 1402-1415.
- [13] S. Javadov, M. Karmazyn, N. Escobales, Mitochondrial Permeability Transition Pore Opening as a Promising Therapeutic Target in Cardiac Diseases, *Journal of Pharmacology and Experimental Therapeutics*, 330 (2009) 670-678.
- [14] J.N. Weiss, P. Korge, H.M. Honda, P. Ping, Role of the Mitochondrial Permeability Transition in Myocardial Disease, *Circulation research*, 93 (2003) 292-301.
- [15] R.J. White, I.J. Reynolds, Mitochondrial depolarization in glutamate-stimulated neurons: an early signal specific to excitotoxin exposure, *The Journal of neuroscience : the official journal of the Society for Neuroscience*, 16 (1996) 5688-5697.
- [16] L.J. Martin, S. Semenkow, A. Hanaford, M. Wong, Mitochondrial permeability transition pore regulates Parkinson's disease development in mutant alpha-synuclein transgenic mice, *Neurobiology of aging*, 35 (2014) 1132-1152.
- [17] M.D. Norenberg, K.V.R. Rao, The mitochondrial permeability transition in neurologic disease, *Neurochemistry International*, 50 (2007) 983-997.
- [18] V. Calabrese, G. Scapagnini, A.M. Giuffrida Stella, T.E. Bates, J.B. Clark, Mitochondrial Involvement in Brain Function and Dysfunction: Relevance to Aging, *Neurodegenerative Disorders and Longevity*, *Neurochem Res*, 26 (2001) 739-764.
- [19] L.J. Martin, B. Gertz, Y. Pan, A.C. Price, J.D. Molkenkin, Q. Chang, The mitochondrial permeability transition pore in motor neurons: Involvement in the pathobiology of ALS mice, *Experimental Neurology*, 218 (2009) 333-346.
- [20] A. Rasola, P. Bernardi, The mitochondrial permeability transition pore and its involvement in cell death and in disease pathogenesis, *Apoptosis : an international journal on programmed cell death*, 12 (2007) 815-833.
- [21] A.L. King, T.M. Swain, Z. Mao, U.S. Udoh, C.R. Oliva, A.M. Betancourt, C.E. Griguer, D.R. Crowe, M. Lesort, S.M. Bailey, Involvement of the mitochondrial permeability transition pore in chronic ethanol-mediated liver injury in mice, *American journal of physiology. Gastrointestinal and liver physiology*, 306 (2014) G265-277.
- [22] Y. Masubuchi, C. Suda, T. Horie, Involvement of mitochondrial permeability transition in acetaminophen-induced liver injury in mice, *Journal of hepatology*, 42 (2005) 110-116.
- [23] L. Dalla Via, A.N. Garcia-Argaez, M. Martinez-Vazquez, S. Grancara, P. Martinis, A. Toninello, Mitochondrial permeability transition as target of anticancer drugs, *Current pharmaceutical design*, 20 (2014) 223-244.
- [24] V.K. Rao, E.A. Carlson, S.S. Yan, Mitochondrial permeability transition pore is a potential drug target for neurodegeneration, *Biochimica et biophysica acta*, 1842 (2014) 1267-1272.
- [25] K. Boengler, D. Hilfiker-Kleiner, G. Heusch, R. Schulz, Inhibition of permeability transition pore opening by mitochondrial STAT3 and its role in myocardial ischemia/reperfusion, *Basic research in cardiology*, 105 (2010) 771-785.

- [26] C. Martel, L.H. Huynh, A. Garnier, R. Ventura-Clapier, C. Brenner, Inhibition of the Mitochondrial Permeability Transition for Cytoprotection: Direct versus Indirect Mechanisms, *Biochemistry Research International*, 2012 (2012) 13.
- [27] R.A. Haworth, D.R. Hunter, The Ca²⁺-induced membrane transition in mitochondria, *Archives of Biochemistry and Biophysics*, 195 (1979) 460-467.
- [28] G. Morciano, C. Giorgi, M. Bonora, S. Punzetti, R. Pavesini, M.R. Wieckowski, G. Campo, P. Pinton, Molecular identity of the mitochondrial permeability transition pore and its role in ischemia-reperfusion injury, *Journal of Molecular and Cellular Cardiology*, 78 (2015) 142-153.
- [29] S. Javadov, A. Kuznetsov, Mitochondrial Permeability Transition and Cell Death: The Role of Cyclophilin D, *Frontiers in Physiology*, 4 (2013) 76.
- [30] C.P. Baines, R.A. Kaiser, N.H. Purcell, N.S. Blair, H. Osinska, M.A. Hambleton, E.W. Brunskill, M.R. Sayen, R.A. Gottlieb, G.W. Dorn, J. Robbins, J.D. Molkenin, Loss of cyclophilin D reveals a critical role for mitochondrial permeability transition in cell death, *Nature*, 434 (2005) 658-662.
- [31] N. Fournier, G. Ducet, A. Crevat, Action of cyclosporine on mitochondrial calcium fluxes, *Journal of bioenergetics and biomembranes*, 19 (1987) 297-303.
- [32] M. Crompton, H. Ellinger, A. Costi, Inhibition by cyclosporin A of a Ca²⁺-dependent pore in heart mitochondria activated by inorganic phosphate and oxidative stress, *The Biochemical journal*, 255 (1988) 357-360.
- [33] A. Laupacis, P.A. Keown, R.A. Ulan, N. McKenzie, C.R. Stiller, Cyclosporin A: a powerful immunosuppressant, *Canadian Medical Association Journal*, 126 (1982) 1041-1046.
- [34] P. Bellwon, M. Culot, A. Wilmes, T. Schmidt, M.G. Zurich, L. Schultz, O. Schmal, A. Gramowski-Voss, D.G. Weiss, P. Jennings, A. Bal-Price, E. Testai, W. Dekant, Cyclosporine A kinetics in brain cell cultures and its potential of crossing the blood-brain barrier, *Toxicology in vitro : an international journal published in association with BIBRA*, 30 (2015) 166-175.
- [35] A. Zulian, E. Rizzo, M. Schiavone, E. Palma, F. Tagliavini, B. Blaauw, L. Merlini, N.M. Maraldi, P. Sabatelli, P. Braghetta, P. Bonaldo, F. Argenton, P. Bernardi, NIM811, a cyclophilin inhibitor without immunosuppressive activity, is beneficial in collagen VI congenital muscular dystrophy models, *Human molecular genetics*, 23 (2014) 5353-5363.
- [36] M.J. Hansson, G. Mattiasson, R. Mansson, J. Karlsson, M.F. Keep, P. Waldmeier, U.T. Ruegg, J.M. Dumont, K. Besseghir, E. Elmer, The nonimmunosuppressive cyclosporin analogs NIM811 and UNIL025 display nanomolar potencies on permeability transition in brain-derived mitochondria, *Journal of bioenergetics and biomembranes*, 36 (2004) 407-413.
- [37] H.-x. Guo, F. Wang, K.-q. Yu, J. Chen, D.-l. Bai, K.-x. Chen, X. Shen, H.-l. Jiang, Novel cyclophilin D inhibitors derived from quinoxaline exhibit highly inhibitory activity against rat mitochondrial swelling and Ca²⁺ uptake/release, *Acta Pharmacol Sin*, 26 (2005) 1201-1211.
- [38] S. Murasawa, K. Iuchi, S. Sato, T. Noguchi-Yachide, M. Sodeoka, T. Yokomatsu, K. Dodo, Y. Hashimoto, H. Aoyama, Small-molecular inhibitors of Ca²⁺-induced mitochondrial permeability transition (MPT) derived from muscle relaxant dantrolene, *Bioorganic & Medicinal Chemistry*, 20 (2012) 6384-6393.
- [39] S. Roy, J. Šileikytė, M. Schiavone, B. Neuenswander, F. Argenton, J. Aubé, M.P. Hedrick, T.D.Y. Chung, M.A. Forte, P. Bernardi, F.J. Schoenen, Discovery, Synthesis, and Optimization of Diarylisoxazole-3-carboxamides as Potent Inhibitors of the Mitochondrial Permeability Transition Pore, *ChemMedChem*, 10 (2015) 1655-1671.
- [40] S. Roy, J. Šileikytė, B. Neuenswander, M.P. Hedrick, T.D.Y. Chung, J. Aubé, F.J. Schoenen, M.A. Forte, P. Bernardi, N-Phenylbenzamides as Potent Inhibitors of the Mitochondrial Permeability Transition Pore, *ChemMedChem*, 11 (2016) 283-288.

- [41] Y.S. Kim, S.H. Jung, B.G. Park, M.K. Ko, H.S. Jang, K. Choi, J.H. Baik, J. Lee, J.K. Lee, A.N. Pae, Y.S. Cho, S.J. Min, Synthesis and evaluation of oxime derivatives as modulators for amyloid beta-induced mitochondrial dysfunction, *European journal of medicinal chemistry*, 62 (2013) 71-83.
- [42] S. Jung, K. Choi, A.N. Pae, J.K. Lee, H. Choo, G. Keum, Y.S. Cho, S.J. Min, Facile diverted synthesis of pyrrolidinyl triazoles using organotrifluoroborate: discovery of potential mPTP blockers, *Organic & biomolecular chemistry*, 12 (2014) 9674-9682.
- [43] A. Elkamhawy, J.-e. Park, A.H.E. Hassan, H. Ra, A.N. Pae, J. Lee, B.-G. Park, B. Moon, H.-M. Park, E.J. Roh, Discovery of 1-(3-(benzyloxy)pyridin-2-yl)-3-(2-(piperazin-1-yl)ethyl)urea: A new modulator for amyloid beta-induced mitochondrial dysfunction, *European journal of medicinal chemistry*, 128 (2017) 56-69.
- [44] K. Kajitani, M. Fujihashi, Y. Kobayashi, S. Shimizu, Y. Tsujimoto, K. Miki, Crystal structure of human cyclophilin D in complex with its inhibitor, cyclosporin A at 0.96-Å resolution, *Proteins*, 70 (2008) 1635-1639.
- [45] S. Ni, Y. Yuan, J. Huang, X. Mao, M. Lv, J. Zhu, X. Shen, J. Pei, L. Lai, H. Jiang, J. Li, Discovering Potent Small Molecule Inhibitors of Cyclophilin A Using de Novo Drug Design Approach, *Journal of Medicinal Chemistry*, 52 (2009) 5295-5298.
- [46] S. Liu, A.M. Crider, C. Tang, B. Ho, M. Ankersen, C.E. Stidsen, 2-pyridylthioureas: novel nonpeptide somatostatin agonists with SST4 selectivity, *Current pharmaceutical design*, 5 (1999) 255-263.
- [47] M. Reers, T.W. Smith, L.B. Chen, J-aggregate formation of a carbocyanine as a quantitative fluorescent indicator of membrane potential, *Biochemistry*, 30 (1991) 4480-4486.
- [48] S.T. Smiley, M. Reers, C. Mottola-Hartshorn, M. Lin, A. Chen, T.W. Smith, G.D. Steele, L.B. Chen, Intracellular heterogeneity in mitochondrial membrane potentials revealed by a J-aggregate-forming lipophilic cation JC-1, *Proceedings of the National Academy of Sciences*, 88 (1991) 3671-3675.
- [49] E.A.G. Blomme, Y. Will, *Toxicology Strategies for Drug Discovery: Present and Future*, *Chemical Research in Toxicology*, 29 (2016) 473-504.
- [50] S. Nadanaciva, Y. Will, *Current Concepts in Drug-Induced Mitochondrial Toxicity*, in: *Current Protocols in Toxicology*, John Wiley & Sons, Inc., 2001.
- [51] K. Chan, D. Truong, N. Shangari, P.J. O'Brien, Drug-induced mitochondrial toxicity, *Expert Opinion on Drug Metabolism & Toxicology*, 1 (2005) 655-669.
- [52] R. Kaye, C.A. Lasagna-Reeves, Molecular mechanisms of amyloid oligomers toxicity, *Journal of Alzheimer's disease : JAD*, 33 Suppl 1 (2013) S67-78.
- [53] P. Cizas, A. Jekabsone, V. Borutaite, R. Morkuniene, Prevention of amyloid-beta oligomer-induced neuronal death by EGTA, estradiol, and endocytosis inhibitor, *Medicina (Kaunas, Lithuania)*, 47 (2011) 107-112.
- [54] C. Barucker, H.J. Bittner, P.K.Y. Chang, S. Cameron, M.A. Hancock, F. Liebsch, S. Hossain, A. Harmeier, H. Shaw, F.M. Charron, M. Gensler, P. Dembny, W. Zhuang, D. Schmitz, J.P. Rabe, Y. Rao, R. Lurz, P.W. Hildebrand, R.A. McKinney, G. Multhaup, A β 42-oligomer Interacting Peptide (AIP) neutralizes toxic amyloid- β 42 species and protects synaptic structure and function, *Scientific Reports*, 5 (2015) 15410.
- [55] M. Taufer, M. Crowley, D.J. Price, A.A. Chien, C.L. Brooks, Study of a highly accurate and fast protein-ligand docking method based on molecular dynamics, *Concurrency and Computation: Practice and Experience*, 17 (2005) 1627-1641.
- [56] G. Wu, D.H. Robertson, C.L. Brooks, 3rd, M. Vieth, Detailed analysis of grid-based molecular docking: A case study of CDOCKER-A CHARMM-based MD docking algorithm, *Journal of computational chemistry*, 24 (2003) 1549-1562.

Tables**Table 1.** *In vitro* blocking activity of the new thioureas against A β -induced mPTP opening in hippocampal neuronal cell line HT-22 (JC-1 assay) at dose of 5 μ M

Cpd	X	R ¹	R ²	Increased g/r ratio (%) ^{a,b}	Cpd	X	R ¹	R ²	Increased g/r ratio (%) ^{a,b}
9a	CH	H	ethyl	66.8	9o	CH	2-Cl	4-methylphenyl	13.0
9b	CH	H	isopropyl	45.2	9p	CH	2-Cl	1-naphthyl	17.5
9c	CH	H	<i>tert</i> -butyl	91.0	9q	CH	3-Cl	<i>tert</i> -butyl	112.0
9d	CH	H	benzyl	75.3	9r	CH	3-Cl	3-chlorophenyl	38.0
9e	CH	H	3-chlorophenyl	25.3	9s	CH	3-Cl	4-methylphenyl	26.0
9f	CH	H	4-methylphenyl	23.3	9t	CH	3-Cl	1-naphthyl	26.0
9g	CH	H	1-naphthyl	17.1	9u	N	3-F	isopropyl	43.1
9h	CH	3-F	ethyl	88.7	9v	N	3-F	<i>tert</i> -butyl	28.1
9i	CH	3-F	isopropyl	86.0	9w	N	3-F	4-methylphenyl	4.6
9j	CH	3-F	<i>tert</i> -butyl	123.4	9x	N	2-Cl	isopropyl	56.3
9k	CH	3-F	1-naphthyl	16.7	9y	N	2-Cl	benzyl	5.3
9l	CH	2-Cl	ethyl	94.1	9z	N	2-Cl	3-chlorophenyl	30.8
9m	CH	2-Cl	isopropyl	31.7	CsA	–	–	–	46.0
9n	CH	2-Cl	3-chlorophenyl	14.2					

^a % Increase of fluorescence-ratio (green/red) after treatment of each compound and A β with regard to that of A β alone (100%). See the text for more detailed information.

^b All data are reported as the average of duplicates.

Table 2. Results of evaluation of compounds-induced deterioration of mitochondrial energy production and neuronal cells viability

Cpd	ATP Production (%) ^a	Cell viability (%) ^b	Protection against A β induced neurotoxicity (%) ^c	Cpd	ATP Production (%) ^a	Cell viability (%) ^b	Protection against A β induced neurotoxicity (%) ^c
9e	68.0	ND ^d	ND ^d	9s	94.5	96.2	22.8
9f	66.0	ND ^d	ND ^d	9t	107.4	123.3	18.6
9g	65.0	ND ^d	ND ^d	9v	99.7	100.8	13.2
9k	100.3	102.5	48.2	9w	101.5	96.4	69.3
9m	93.7	99.3	-6.7	9y	85.1	104.7	3.8
9n	102.7	115.7	22.7	9z	98.0	113.6	29.6
9o	101.9	93.5	6.6	Piracetam	88	132	29.0
9p	100.3	89.3	9.5	CsA	ND ^d	90	ND ^d
9r	104.0	98.3	51.8				

^a % ATP production in hippocampal neuronal cell line HT-22 calculated after 7 hours incubation with 5 μ M of each compound.

^b % MTT-cell viability of hippocampal neuronal cell line HT-22 after 24 hours incubation with at 5 μ M of each compound.

^c % hippocampal HT-22 cells remaining viable in A β -induced cytotoxicity assay after 24 hours of incubation with 5 μ M concentrations of both of A β and each tested compound.

^d ND not determined.

Figures

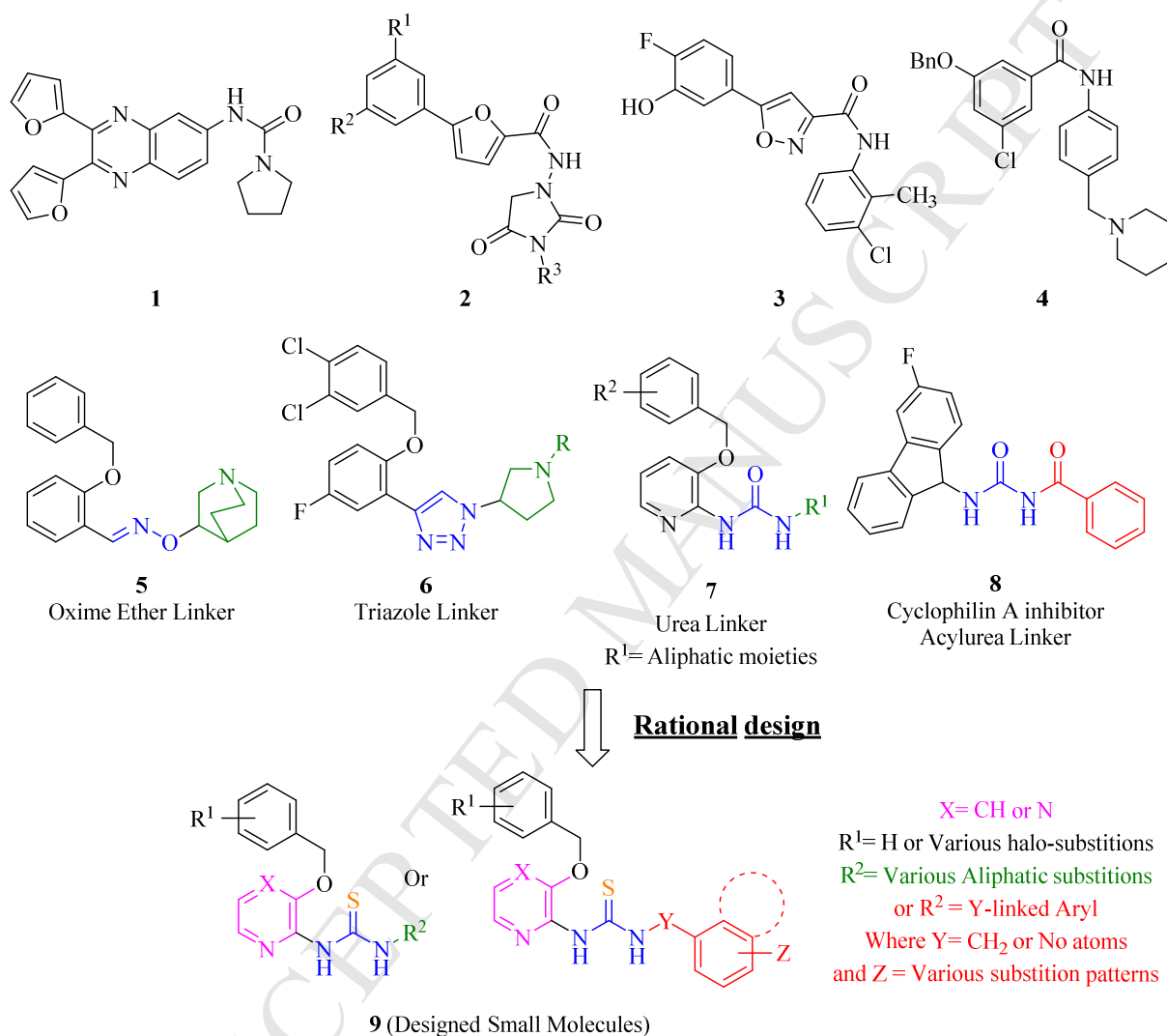
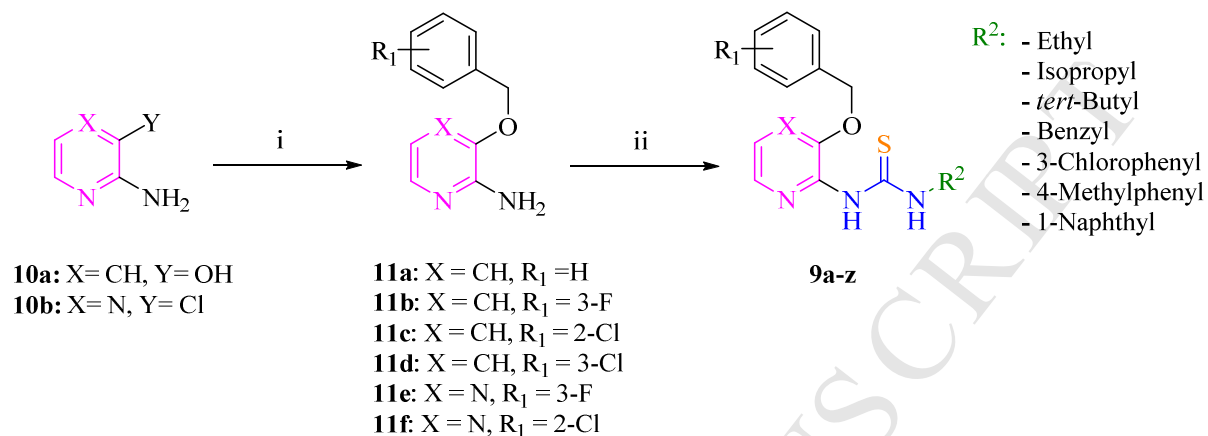


Fig. 1. Reported small molecules with mPTP inhibition activity and Design of small molecules mPTP inhibitors *via* replacing the linker, modifying the eastern moiety and retaining pyridine or replacement with isosteric pyrazine in the aromatic moiety.



Scheme 1. Reagents and conditions: (i) for derivatives **11b–d**: to **10a** starting material: 1) NaOH, H₂O, Bu₄NBr, DCM, rt, 15 min. 2) appropriate benzylbromide, DCM, rt, 18 h; for derivatives **11e–f**: to **10b** starting material: NaH (60% in mineral oil), appropriate benzyl alcohol derivative, DMF, 100 °C, 15 h. (ii) for aliphatic thiourea derivatives: appropriate aliphatic isothiocyanate derivative, NaH (60% in mineral oil), THF, reflux, 5–18 h; for aromatic thiourea derivatives: appropriate aromatic isothiocyanate derivative, THF, reflux, 3–6 h.

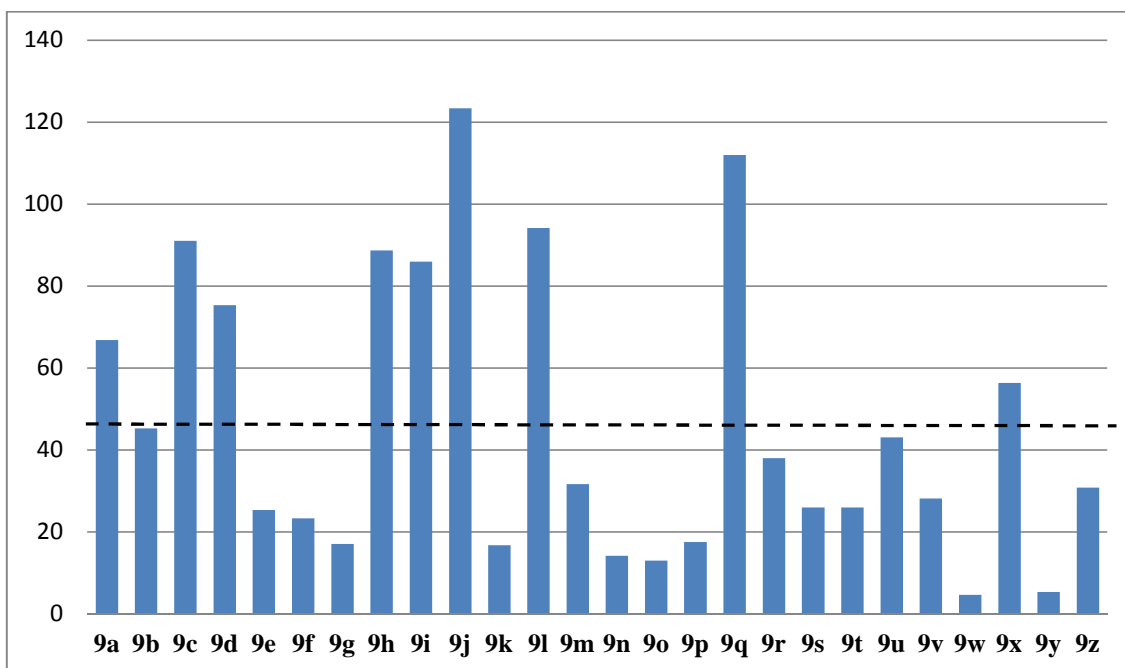


Fig. 2. Percentage increase in the fluorescence ratio (green/red) after treatment with tested compounds and A β with respect to that of A β alone (100%). Dashed line represents fluorescence ratio of Cyclosporin A (CsA) used as a control.

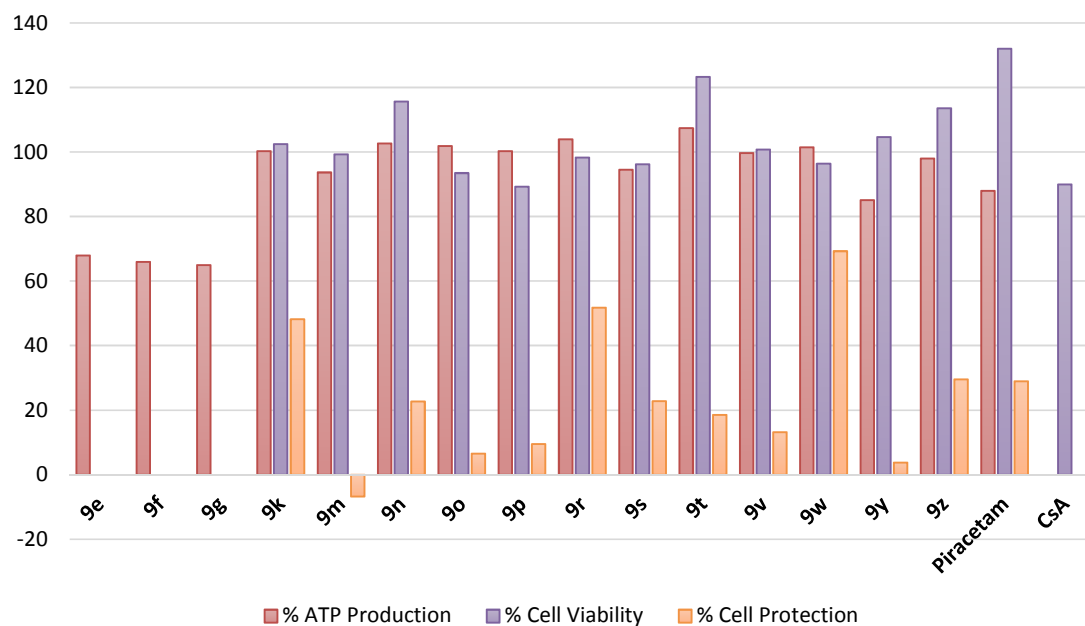


Fig. 3. The effect of 5 μ M concentration of each tested compound on ATP production and cell viability, in addition to, the percentage of protective effect against neurocytotoxicity induced by 5 μ M concentration of $A\beta$.

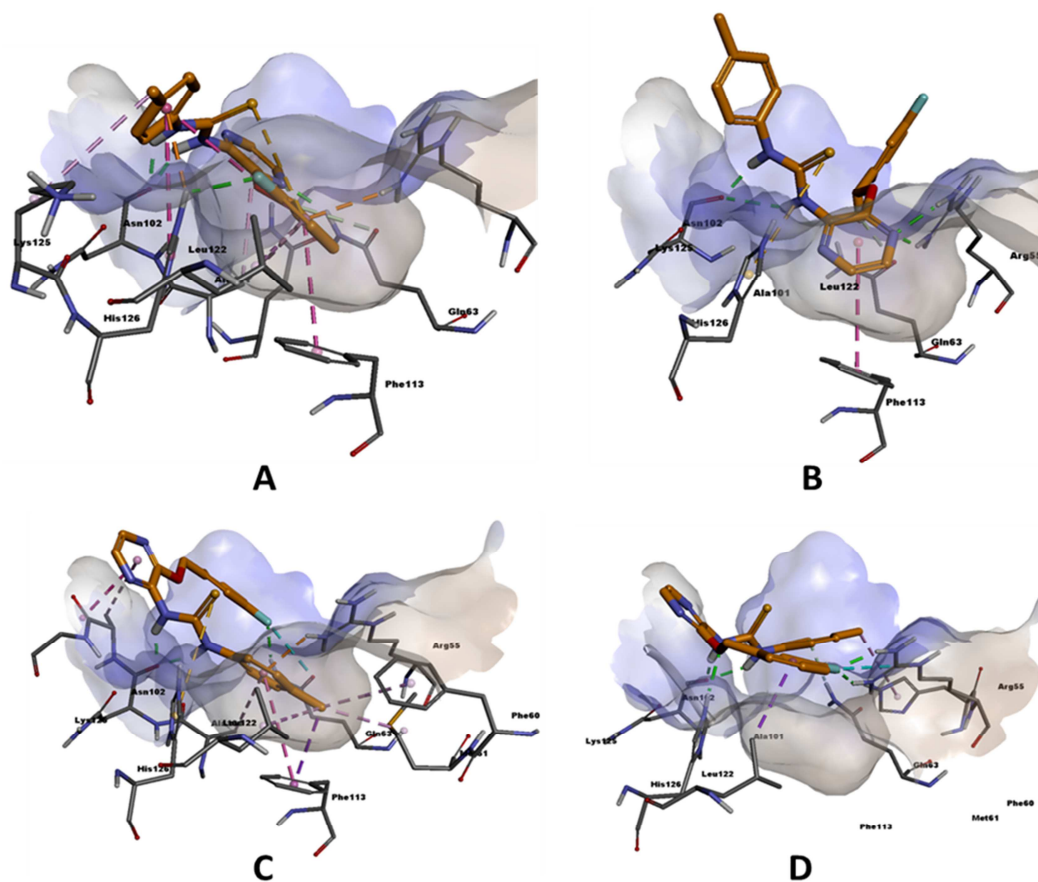


Fig. 4. Different Binding patterns of compound **9w**; A) Binding mode 1 subtype 1; in which the aromatic ring of the benzyloxy moiety docks into the hydrophobic pocket 1. B) Binding mode 1 subtype 2; in which the central pyrazine ring docks into the hydrophobic pocket 1. C) Binding mode 1 subtype 3; in which the eastern aromatic moiety docks into the hydrophobic pocket 1. D) Binding mode 2; in which the hydrophobic pocket 1 is vacant while compound **9w** is docked above it.

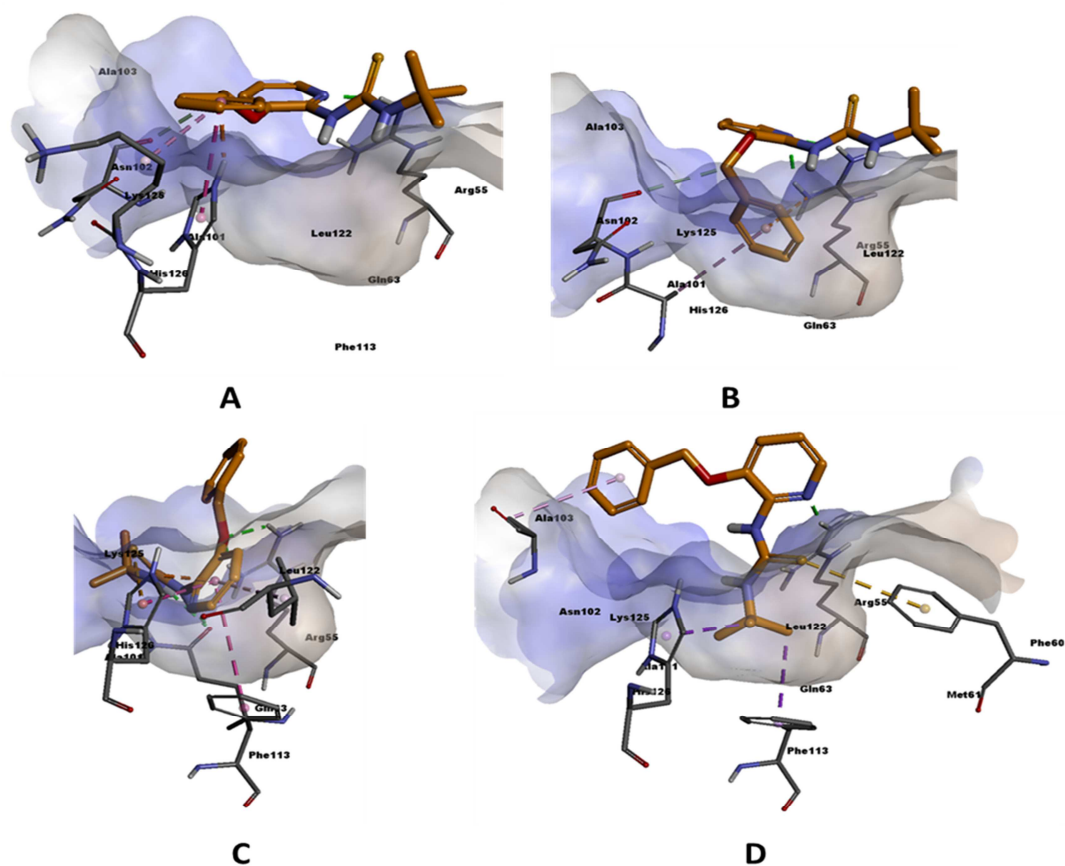


Fig. 5. The best poses of different binding modes of the inefficient mPTP blocker compound **9c**; A) Compound **9c** showing binding mode 2; in which the hydrophobic pocket 1 is vacant while compound **9c** is docked above it. B) Compound **9c** showing binding mode 1 subtype 1; in which the aromatic ring of the benzyloxy moiety docks into the hydrophobic pocket 1. C) Compound **9c** showing binding mode 1 subtype 2; in which the central pyridine ring docks into the hydrophobic pocket 1. D) Compound **9c** showing binding mode 1 subtype 3; in which the eastern hydrophobic moiety docks into the hydrophobic pocket 1.

Highlights

- Biological activity of seventeen compounds against A β -induced mPTP opening was superior to that of Cyclosporin A.
- Derivatives **9w**, **9r**, and **9k** had safe profile regarding ATP production and cell viability.
- Molecular modeling study predicted plausible binding modes explaining the elicited mPTP blocking activity.
- This study suggests compounds **9w**, **9r**, and **9k** as leads for further development of novel therapy to Alzheimer's disease.